Milieu en Natuur Planbureau

MNP report 555034001/2006

Monitoring aerosol concentrations and optical thickness over Europe

PARMA final report

R.B.A. Koelemeijer, M. Schaap*,
R.M.A. Timmermans*, C.D. Homan,
J. Matthijsen, J. van de Kassteele, and
P.J.H. Builtjes*

* TNO Bouw en Ondergrond

Contact:
Robert Koelemeijer
Milieu- en Natuurplanbureau (MNP)
Robert.Koelemeijer@mnp.nl

This investigation has been funded in part by the Netherlands Agency for Aerospace Programmes (NIVR), within the framework of project E/555034/01, Monitoring particulate matter for climate and health effects in Europe (PARMA), NIVR project code 53410 RI.

Netherlands Environmental Assessment Agency (MNP), P.O. Box 303, 3720 AH Bilthoven,
telephone: + 31 30 274 2745; www.mnp.nl

Rapport in het kort

Monitoring van aerosolconcentraties en optische dikte in Europa
PARMA eindrapport

Het vergelijken van fijnstofconcentraties tussen verschillende Europese landen wordt bemoeilijkt doordat in Europa diverse meetmethoden worden gehanteerd. In dit rapport zijn, naast deze meetgegevens van fijn stof, gegevens van de MODIS satelliet en modelberekeningen gebruikt om kaarten van fijn stof ($PM_{2.5}$) in Europa te verbeteren. Twee methoden zijn daarbij gebruikt: een statistische methode en een data-assimilatiemethode. In het algemeen komen de ruimtelijke gradiënten van $PM_{2.5}$ volgens beide methodieken behoorlijk goed overeen in Noordwest-Europa. De hoogste fijnstofconcentraties worden gevonden in drukbevolkte en geïndustrialiseerde gebieden, zoals de Po-vlakte, de Benelux-landen, het Ruhrgebied, gebieden in Centraal-Europa en diverse grote steden in Europa. De grootste onzekerheden in de data-assimilatiemethode zijn gerelateerd aan bronnen van aerosolen die niet in modellen worden meegenomen, en aan optische eigenschappen van aerosolen.

Contents

Executive summary

The understanding of particulate matter levels over Europe as a whole is at present limited by the diversity of ground level measurement methods. This hampers a comparison of air quality levels between EU member states, and checking compliance with (proposed) EU limit values. In this study, satellite observations (MODIS) of aerosol optical thickness (AOT) have been used to improve the mapping of yearly average $PM_{2.5}$ concentrations in Europe in 2003. Two different approaches were followed to use AOT data for $PM_{2.5}$ mapping: a statistical approach and a data-assimilation approach. The AOT measurements from MODIS were first validated against AERONET data.

AOT validation results
The AOT data measured by the MODIS instruments on board of the EOS/Terra and EOS/Aqua platforms, have been compared to AOT measurements of the AERONET surface network. The spatial correlation between MODIS and AERONET observed yearly average AOT over Europe is 0.64, and 0.72 using the fraction of the MODIS derived AOT pertaining to small particles only (AOT_F). The temporal correlation between MODIS and AERONET observed AOT is generally high, with a mean correlation of 0.72 (0.77 median of all stations), with slightly lower correlation for the AOT_F. However, the results show that MODIS systematically overestimates the AOT. On average, the annual mean AOT (AOT_F) observed by MODIS averaged over all validation stations is 0.30 (0.25) compared to 0.20 as obtained by the sun-photometers. A more or less constant bias was found between MODIS AOT and AOT_F and AERONET, of 0.7 and 0.9, respectively. After correction of the AOT and AOT_F values, through multiplication with 0.7 and 0.9, respectively, the MODIS data agree with AERONET within the uncertainty range of $\pm 0.05 \pm 0.2 AOT_F$.

Statistical mapping results
A map of yearly average concentrations of $PM_{2.5}$ has been constructed, through fitting modelled $PM_{2.5}$ (with the Lotos-Euros model) and measured AOT_F fields to observed $PM_{2.5}$ concentrations. For this fitting, in the final stage of this study, also five EMEP stations were added to the eight rural background stations in the AirBase database, to obtain a more uniform spatial coverage within the fitting domain (Europe). Using both modelled $PM_{2.5}$ and measured AOT_F fields as explanatory variables for the yearly average $PM_{2.5}$ distribution, the RMS-errors decrease by about 25% compared to fitting with only one explanatory variable. The spatial correlation between fitted and observed yearly average $PM_{2.5}$ levels is 0.82, with a RMS-error of 2.8 $\mu g/m^3$. Since the modelled $PM_{2.5}$ and measured AOT_F fields contribute about equally to the fitted map, the fitted map resembles the features of the modelled $PM_{2.5}$ map and the AOT_F map in equal proportions. The number of stations considered in this fitting is limited however, and adding more stations may significantly alter the resulting map, depending on where these stations are located. For example, the gradient in AOT_F between Scandinavia and Spain appears not very realistic, with higher AOT_F-values in Scandinavia than in Spain. This gradient is opposite (and more realistic) in the modelled field. Therefore, adding more stations in Scandinavia and Spain will reduce the weight attached to the AOT_F-field and increase that attached to the modelled field.

Assimilation results
The assimilation was performed with a LOTOS-EUROS model version that was slightly updated to that used in the statistical approach. Also, the assimilation has been done for a more limited area to speed up calculation time. The assimilation of MODIS AOT_F in

LOTOS-EUROS leads to AOT fields that are in better agreement with the AERONET measurements. Through assimilation, the timing and representation of spatial patterns in AOT improves substantially. Through the assimilation of MODIS AOT_F, $PM_{2.5}$ levels are increased by 2-3 microgram in central Europe, but, as a result of the assimilation method applied, less in regions closer to the model boundaries. The assimilation slightly increases the spatial correlation between measured and modelled yearly average $PM_{2.5}$ (from 0.88 to 0.91).

In the assimilation, the emissions (primary and precursors of secondary aerosols) have been taken as free parameter. Therefore, as a result of the assimilation, changes in the emission strengths are found. However, not much value was attributed to this, as the differences between modelled and measured AOT are large, and these differences between modelled and measured AOT are not only attributable to uncertainties in emissions of aerosols and their precursors from known sources. The differences also stem from emissions that are not taken into account in the emission inventories (like windblown dust), and errors in the description in the chemical transformation, dispersion and deposition of aerosols. Moreover, there is a large uncertainty in the optical properties of the aerosols that determine the relationship between PM and AOT, which explains part of the differences between measured and modelled AOT values.

Comparison between statistical mapping and assimilation

Generally, the spatial features in the map based on the statistical mapping approach resemble that of the assimilation approach in the central part of the model domain (North-West Europe). It is apparent that the assimilation approach leads to lower $PM_{2.5}$ concentrations than the statistical mapping approach. The absolute difference is 2-3 $\mu g/m^3$ in the centre of the domain and it increases to 5-7 $\mu g/m^3$ near the boundaries of the domain. The reason is that in the statistical mapping approach, the absolute measured levels of the $PM_{2.5}$ are actively used in the mapping procedure, in contrast to the assimilation approach where $PM_{2.5}$ measurements are used only for validation. Because of this, the statistical mapping approach leads by definition to almost no bias compared to the ground-based measurements, while data-assimilation will provide a bias depending on the model underestimation of PM, the uncertainty in the conversion between AOT and PM, and the uncertainty assumed for the AOT data and model results.

Both methods lead to a better description of the spatial gradients in the yearly average $PM_{2.5}$ field in Europe as compared to modelled results only. In the assimilation approach, the spatial correlation between yearly average $PM_{2.5}$ measurements and the assimilated $PM_{2.5}$ field was already high (0.88) in the area considered, and increases to 0.91 after assimilation, while in the statistical approach, which is applied to a larger domain and with a slightly different model version, it increases from 0.70 to 0.82. Highest concentrations of particulate matter are found in densely populated and industrialized areas, such as the Po-valley, the Benelux countries, the Ruhr area, areas in Central Europe and specific large cities in Europe. Largest uncertainties in both methods are related to missing aerosol sources and the optical properties of aerosols that determine the relation between AOT and PM.

1. Introduction

In Europe, particulate matter (PM), expressed as aerosol mass concentrations at the surface, is the most important air pollutant responsible for loss of human health. Short term exposure to particulate matter has frequently been associated with increased morbidity (cardiovascular and respiratory disease) and mortality (e.g., Brunekreef and Holgate, 2002). It is estimated that short-term exposure to particulate matter in the Netherlands at present levels leads to 1000 - 2000 premature deaths per year (Knol and Staatsen, 2005), with an average lifetime reduction of a few days to a few months. Effects of long-term exposure to particulate matter are much more uncertain than the short-term effects, but are believed to have a much greater effect on health loss (Dockery et al., 1993; Pope et al., 1995; Pope et al., 2002). Estimates of the mortality number for the Netherlands caused by long-term exposure to particulate matter amount to ten-thousand to several ten-thousands premature deaths per year, with a reduction of life-time of several years, although, as mentioned, the epidemiological evidence base for these effects is still limited (Knol and Staatsen, 2005).

The understanding of PM concentrations levels and monitoring of compliance with the EU limit values would greatly benefit from consistent and accurate PM maps covering the whole of Europe. At present all EU member states perform air quality measurements to check compliance with the limit values. Although these ground-based measurements may be relatively precise, they are only representative for a limited area because aerosol sources vary over small spatial scales and the aerosol lifetime is of the order of less than an hour to several days, depending on particle size and chemical composition. Furthermore, it is widely recognized that it is problematic to measure the absolute level of PM on a routine basis. In routine measurement processes, heating of the air sample is necessary, which gives rise to (partial) volatilization of semi-volatile components. This in turn leads to systematic measurement errors depending on the measurement technique used and aerosol composition. The limited spatial representativeness and different systematic errors of over 25 national air quality networks make it virtually impossible to achieve an overview across Europe based on ground-based measurements only. Model calculations can be of some help by applying for instance data assimilation. The quality of the necessary emission data are however seriously hampering models to generate useful information. Anthropogenic sources are in general not very accurately known and the contribution from natural sources is hard to quantify, due to limited knowledge of the emission process and quantity.

Satellite measurements are less precise than ground level observations, but provide full spatial coverage and are – in principle – consistent for the whole European region. This suggests that satellite measurements may be useful to improve the insight in PM distributions in Europe in combination with models and ground based measurements. Various studies in the U.S. have reported good correlations between satellite derived AOT and $PM_{2.5}$ surface concentration measurements in parts of the U.S. (Wang et al., 2003; Hutchison, 2003). In general, promising correlations are found between one-month time-series of AOT and $PM_{2.5}$ for many stations in the Eastern and Midwest U.S. Other stations, however, particularly in the Western US, show hardly any correlation (Engel-Cox et al., 2004). Variations in local meteorological conditions, occurrence of multiple aerosol layers, and variations in aerosol chemical composition likely play an important role in determining the strengths of such correlations. For a location in Europe (the Aeronet station at Ispra, Northern Italy), Chu et al. (2003) have shown that time-series of AOT and 24-h average PM_{10} measurements correlate

well, for a period of several months in 2001 with stable meteorological conditions. This suggests that AOT observations may be useful to improve mapping of PM concentrations.

Besides air quality, aerosols also affect the environment by modifying the radiative budget of the Earth (direct and indirect radiative forcing). On the global scale, fossil fuel combustion is the main contributor (>60%) to total anthropogenic aerosol emissions. Because the sources of aerosols that affect climate and human health are the same, these problems are tightly linked. Recent estimates of direct radiative forcing by 'reflective' aerosols (sulphates, ammonium nitrate, and organic aerosols resulting from biomass burning, fossil fuel combustion and atmospheric oxidation of volatile organic compounds) amount to -1 to -1.5 W/m^2 globally averaged (IPCC, 2001; Hansen and Sato, 2001), compared to a positive forcing of +2.5 W/m^2 by the well-mixed greenhouse gases. Absorption of solar radiation by aerosols is primarily due to black carbon (soot) aerosols, resulting from incomplete combustion of fossil fuels and biomass, and is estimated to exert a forcing of +0.25 to +0.5 W/m^2. The effect of aerosols on cloud properties (indirect radiative forcing) is even more uncertain. IPCC (2001) estimates a net forcing of -1 W/m^2, with an uncertainty of at least a factor of 2. These numbers are estimates at the global scale; regional forcings and their uncertainties can be considerably larger.

Both for assessment of exposure of population to $PM_{2.5}$ as well as for assessment of climate forcing by aerosols, reducing uncertainties in emissions and concentrations of aerosols is mandatory. This reports presents the final results of the PARMA project (Monitoring **Par**ticulate **Ma**tter for Climate and Health Effects in Europe), which was aimed at improving the mapping of aerosol optical thickness and $PM_{2.5}$ concentrations, by exploiting ground- and space-based measurements in combination with atmospheric modelling. In this project, the focus has been on mapping $PM_{2.5}$ which is relevant for health effects. In the follow-up project HIRAM (High-resolution Air Quality Monitoring over Europe), more attention will be paid to radiative forcing aspects, and the contribution of several mega-city regions in Europe to aerosol emissions.

In this project, the chemical transport model LOTOS-EUROS, developed by TNO, MNP and RIVM (Schaap et al., 2005a, 2005b) was used. Measurements of aerosol optical thickness (AOT) were used, acquired by the Moderate Resolution Imaging Spectrometer (MODIS) instruments on board the NASA satellite platforms Terra and Aqua in 2003. The AOT satellite measurements have been validated against the independent measurements of AOT by the AERONET ground based network. $PM_{2.5}$ measurements are taken from the EEA air quality database AIRBASE. In this project, improved $PM_{2.5}$ concentrations are derived using two independent approaches:

(1) a statistical mapping approach, involving the MODIS AOT data, ground-based measurements of $PM_{2.5}$ and modelled fields of $PM_{2.5}$, and
(2) a data-assimilation approach, in which MODIS AOT data are assimilated in the LOTOS-EUROS model. In the assimilation (an ensemble Kalman filtering approach), the emissions of aerosols and aerosol precursors are treated as free-parameters and adjusted in the assimilation step such that the modelled and measured AOT values are in closer agreement.

The report is structured as follows. Chapter 2 discusses the theoretical relation between aerosol optical thickness and particulate matter. Primary data sources (MODIS AOT and AirBase $PM_{2.5}$) are discussed in Chapter 3. In Chapter 4, the data-assimilation system for LOTOS-EUROS is described. Results of validation of MODIS AOT with independent AOT

measurements form the AEORNET surface network are described in Chapter 5. In Chapter 6, a comparison is made between spatio-temporal variations in observed AOT and $PM_{2.5}$ in Europe in 2003, and results of the statistical approach to map $PM_{2.5}$ in Europe are presented. In Chapter 7, the results of the data-assimilation approach are presented. In Chapter 8, conclusions are summarized and the results of both approaches to map $PM_{2.5}$ are discussed.

2. Relationship between AOT and PM

In this chapter, the theoretical relationship between the mass concentration of aerosols near the Earth's surface (particulate matter) and (total column) aerosol optical thickness is investigated.

2.1 Definition of optical thickness and Angström-parameter

Aerosols in the atmosphere scatter and absorb solar radiation that is incident on the atmosphere. After interaction with aerosols, the solar beam is attenuated: part of the light is absorbed, and part of it is scattered in all directions. The total effect of scattering and absorption is known as extinction. Since the amount of radiation scattered back to space is dependent on the aerosol optical thickness, the aerosol optical thickness can be derived from satellite measurements of scattered radiation.

Consider a column of air above a surface element which extends from the Earth's surface to the maximum height at which aerosols occur, H. This air column contains aerosols of different sizes, as characterized by their radius r, see figure 2.1.

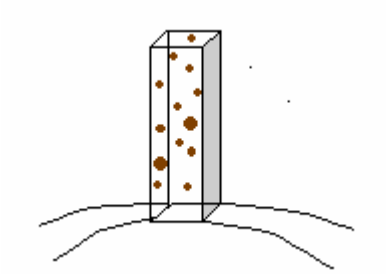

Figure 2.1 Aerosol particles of different size above a surface element. The aerosol optical thickness is the product of the number of particles above the surface element and the average extinction cross-section.

The aerosol (extinction) optical thickness, AOT, of this column is then defined as

$$AOT(\lambda) = \int_0^H \int_0^\infty C_{ext}(r,\lambda)\, n(r,z)\, dr\, dz,$$

where $n(r, z)$ is the aerosol number density as a function of aerosol radius r and height above the surface z, and $C_{ext}(r,\lambda)$ is the extinction cross-section of a particle. Hence, the aerosol optical thickness is a dimensionless quantity, and is the product of the average extinction cross-section for the mixture of aerosol particles (unit: m^{-2}) and the total number of aerosol particles N in an atmospheric column above a surface element (unit: m^2). The extinction cross-section C_{ext} in (2.1) depends on the aerosol particle radius and wavelength of sunlight incident on the particle, λ. The extinction cross-section can be written as

$$C_{ext}(r,\lambda) = G\, Q_{ext}(r,\lambda),$$

where $G = \pi\, r^2$ is the geometrical cross-section of a particle and $Q_{ext}(r,\lambda)$ is the (dimensionless) extinction efficiency. For particles much smaller than the wavelength Q_{ext}

rapidly goes to zero (proportional with r^2), while for particles much larger than the wavelength, Q_{ext} approaches 2. For aerosols with a radius in between these limits, Q_{ext} can be calculated with Mie-theory for spherical particles (van de Hulst, 1981). For particles of intermediate sizes, the function Q_{ext} oscillates and has a maximum near $r = \lambda$, where it can become as large as 4. It follows that C_{ext} approaches zero if the particle radius approaches zero (proportional to r^4, the Rayleigh scattering limit), while for large particles C_{ext} increases with particle radius proportional to πr^2. Also the optical thickness shows this behaviour with particle radius. For realistic aerosol size distributions, this means that the optical thickness is dominated by particles with $0.1 < r < 1$ μm, because these are more abundant than the larger particles and still have relatively large extinction cross-sections.

The scattering properties of aerosols depend on the ratio r/λ,. Hence, the optical thickness depends on the wavelength. This wavelength dependence can be described by the Angström-parameter, α, defined as

$$AOT(\lambda) = AOT(\lambda_0)\left(\frac{\lambda}{\lambda_0}\right)^{-\alpha},$$

where λ_0 indicates a reference wavelength, e.g., 550 nm. The Angström-parameter is a dimensionless number and is typically between 1 and 2 for most mixtures of aerosol particles. The smaller the aerosol particles, the larger their Angström-parameter. Since the MODIS instrument is able to measure optical thickness at multiple wavelengths, the Angström-parameter is derived from MODIS measurements as well, and is used to separate fine and coarse aerosols (see Section 2.2).

2.2 Relation between aerosol optical thickness and mass-concentration at the surface

Below the relation between PM and AOT is derived for a single homogeneous atmospheric layer containing spherical aerosol particles. The mass concentration of aerosols near the surface (unit: μg/m^3), is obtained after drying the sampled air (to avoid humidification of the filter material), and is given by

$$PM = \frac{4}{3}\pi\,\rho \int r^3 n(r)\,dr,$$

where n(r) describes the normalised aerosol size distribution under dry conditions and ρ is the aerosol mass density. The AOT of the layer with height H is given by

$$AOT = \pi \int_0^H \int_0^\infty Q_{ext,amb}(r)\, n_{amb}(r)\, r^2\, dr\, dz = \pi\, f(RH) \int_0^H \int_0^\infty Q_{ext,dry}(r)\, n(r)\, r^2\, dr\, dz,$$

where $n_{amb}(r)$ is the normalised size distribution under ambient relative humidity (*RH*) conditions, $Q_{ext,amb}$ is the extinction efficiency of aerosols under ambient relative humidity conditions, $Q_{ext,dry}$ the extinction efficiency under dry conditions, and *f(RH)* the ratio between these (size-distribution integrated) extinction efficiencies. The function *f(RH)* describes the increase in the extinction efficiency with increasing relative humidity, and depends on the

aerosol hygroscopic properties. In this report the function depicted in figure 2.2 was used, which is based on measurements near the Dutch coast (Veefkind et al., 1996). Similar curves have been reported by Day et al. (2001) for aerosols at various locations in the United States.

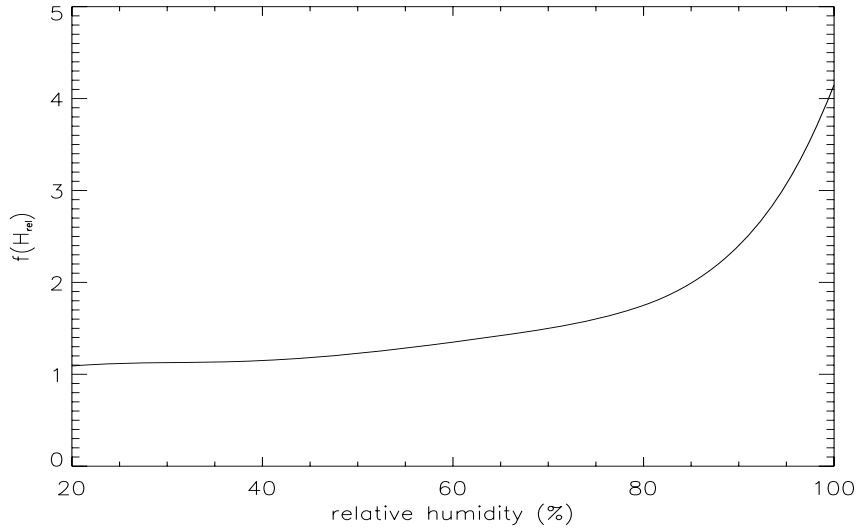

Figure 2.2 Function f(RH) that describes the increase of extinction efficiency (or cross-section) with increasing relative humidity (based on Veefkind et al., 1996).

The size-distribution integrated extinction efficiency is defined as

$$< Q_{ext} >= \frac{\int r^2 Q_{ext}(r) n(r) dr}{\int r^2 n(r) dr},$$

and the effective radius as (Hansen and Travis, 1974)

$$r_{eff} = \frac{\int r^3 (r) n(r) dr}{\int r^2 n(r) dr}$$

Substituting these relations, the following relation between AOT and PM is obtained:

$$AOT = PM \; H \; f(RH) \frac{3 < Q_{ext,dry} >}{4 \rho \, r_{eff}}.$$

Hence, it can be expected that the parameter AOT*=AOT /[*f(RH)* H] correlates better with PM than the AOT directly. Furthermore, it is clear that the aerosol optical thickness and the mass-concentration differ in several respects:

- *Different atmospheric volume*. The aerosol optical thickness is integrated over the total atmospheric column, while the mass-concentration pertains to aerosols near the surface. Thus, in situations of multiple atmospheric layers with substantially different aerosol loadings, the relationship between the two quantities will be weak. If the total aerosol burden is dominated by the concentrations in the boundary layer, their relationship will be stronger. It is estimated that typically about 10 % of the aerosol is found above the boundary layer (Banic et al., 1996; ten Brink et al., 2001, Builtjes et al, 2001).

- *Sensitivity to density.* In contrast to the aerosol optical thickness, the mass concentration is sensitive to the mass density of the aerosol particles itself (ρ), as determined by their chemical composition.
- *Different measurement conditions: ambient versus dry conditions.* The mass-concentration is determined for aerosols under dry conditions, while the aerosol optical thickness is determined under ambient humidity conditions. Hygroscopic aerosols grow in size with increasing relative humidity (see figure 2.2). Larger particles have larger cross-sections, and hence give rise to a larger optical thickness. Hence, the optical thickness is influenced by changes in the relative humidity.
- *Different sensitivity to particle size.* The aerosol optical thickness is proportional to the number of aerosol particles, weighted with their cross-section (proportional with r^2), while the mass-concentration is proportional to the number of aerosol particles weighted with their mass (proportional with r^3). While aerosol particles of any size contribute to the aerosol optical thickness, in practice, the aerosol optical thickness is dominated by particles with $0.1< r< 1$ μm. Mass-concentrations are more dominated by the larger particles in the sample, but only particles are sampled with a radius smaller than r_{max}. For $PM_{2.5}$, r_{max}=1.25 μm and for PM_{10}, r_{max}=5 μm when the atmospheric humidity is low (<50%) or for hydrophobic aerosols. For hygroscopic aerosols in conditions of high atmospheric humidity, the mass-concentration will be more dominated by smaller particles than the same air under dry conditions, because the size-selection is made under ambient conditions, and the mass is determined under dry conditions. Thus, both aerosol optical thickness and $PM_{2.5}$ are generally dominated by particles with r<1 μm.

3. Data sources

Measurements of aerosol optical thickness were obtained from the MODIS instrument on board the Terra and Aqua satellites, which are described in Section 3.1. Daily and hourly averaged particulate matter measurements were extracted from the AirBase database, and are described in Section 3.2.

3.1 Aerosol optical thickness from MODIS

The Moderate-Resolution Imaging Spectroradiometer (MODIS) onboard EOS-Terra satellite was launched into a sun-synchronous polar orbit in December 1999. MODIS makes measurements of sunlight reflected by the Earth's atmosphere and surface, as well as emitted thermal radiation at 36 wavelengths between 0.41 and 14 μm. In May 2002, a second MODIS instrument was launched on board EOS-Aqua. The Terra satellite crosses Europe near 10:30 local solar time (morning orbit), while Aqua crosses Europe near 13:30 local solar time (afternoon orbit). Hence, at least two observations of any place in Europe are obtained per day during daylight hours. Retrieval of aerosol optical thickness (AOT) is restricted to cloud-free conditions, however. The AOT algorithm is completely different and mutually independent for land and sea surfaces. This is because the radiative properties of water and land are very different. The retrieval is more accurate over ocean than over land because the reflection by water is relatively small, homogeneous and well known. The algorithms are described in Kaufman and Tanré (1998), and updates since then are described in Remer et al., 2005. Below the main steps and assumptions in the land algorithm are summarized.

- *Formation of 10x10 km^2 pixels groups.* The retrieval of aerosol optical thickness over land employs primarily three spectral channels centered at wavelengths of 0.47, 0.66, and 2.1 μm. The 0.47 μm and 2.1 μm channels have 500 m resolution. The 0.66 μm channel is degraded from its original resolution of 250 m to 500 m, similar to that of the other two channels. The AOT retrieval then uses ensembles of 20x20 pixels, corresponding to 10x10 km^2 resolution. The resolution of the AOT product is therefore 10x10 km^2.
- *Selection of clear and dark pixels.* The AOT retrieval starts with selecting only cloud free and snow free pixels for each box of 20x20 pixels, using the MODIS cloud mask and Near Real-Time Ice and Snow Extent (NISE) from National Snow and Ice Data Center (NSIDC) and National Center for Environmental Prediction (NCEP) data. Furthermore, only pixels are selected with a measured reflectance at 2.1 μm between 0.01 and 0.25, to avoid very dark (water) and very bright surfaces (unvegetated surfaces, deserts). From the remaining pixels, the darkest 20% and the brightest 50% are discarded, in order to eliminate remaining pixels possibly contaminated by remaining clouds, cloud shadows or bright surfaces (Remer et al., 2005). The remaining pixels are referred to as clear pixels. The average radiance of these pixels is used for the AOT retrieval.
- *Determination of surface reflectance.* The reflectivity measured at 2.1 μm at the top-of-atmosphere is used to infer surface reflectivity at that wavelength. Fine-mode particles (including secondary aerosols, and part of the primary aerosols from traffic and industrial sources, and biomass-burning aerosols), which dominate the AOT in most of Europe, have a negligible optical thickness at 2.1 μm, allowing almost direct observation of the surface (Chu et al., 2003). The surface reflectivity at visible wavelengths is then obtained by assuming a constant ratio between surface reflectivity at 2.1 μm and that at 0.47 μm and 0.66 μm. In reality, this ratio will depend on surface type and its time dependent

characteristics that determine the reflectivity (e.g., vegetation and soil moisture). In the current MODIS algorithm this is not taken into account, and may in principle lead to systematic biases in the AOT depending on surface type and season. Also, the assumption that the aerosol optical thickness is negligible at 2.1 μm no longer holds when the atmosphere contains many large particles, such as wind-blown dust from the surface. Particularly, this may be problematic in semi-arid areas in Southern Europe, that also have frequent episodes of advection of Saharan dust. Therefore, AOT retrievals for these circumstances are restricted to situations where the measured reflectance at 2.1 μm is between 0.15 and 0.25, which is expected to correspond to moderately bright surfaces. In such cases, the AOT error is not very sensitive to the assumed surface reflectance (Remer et al., 2005).

- *Determination of a first-guess aerosol optical thickness.* Based on the measured reflectance and the surface reflectance at 0.47 μm and 0.66 μm, the AOT is derived using a standard look-up table approach. Assuming some 'first-guess' aerosol type, aerosol optical thickness is derived by matching the measured reflectances to values from pre-calculated lookup tables under the same Sun-satellite geometrical conditions and surface reflection. This gives a 'first guess' optical thickness at the two wavelengths.
- *Determination of aerosol optical thickness.* A final retrieval is done similar to the previous step, but now assuming a more realistic aerosol type. This aerosol type is determined from the spectral dependence of the 'first guess' optical thicknesses at 0.47 μm and 0.66 μm. Dust type (dominated by the coarse mode particles) is selected when the first guess' optical thicknesses shows little wavelength dependence. Non-dust types (dominated by fine mode) are selected in case of large wavelength dependence, and mixed types in between. Non-dust models are selected depending on the geographical location; a map can be found in Remer et al. (2005). When the appropriate aerosol model is determined the final aerosol optical thickness is calculated. The aerosol optical thickness at 0.47 and 0.66 μm is interpolated to 0.55 μm, according to the Angstrom-law.

In addition to the AOT, the aerosol optical thickness originating from fine aerosol particles is derived if the aerosol type is mixed. The fine fraction of the AOT, AOT_F, is defined as the fine fraction η times the total aerosol optical thickness:

$$AOT_F = \eta . AOT$$

The parameter η is determined from the spectral dependence of the path radiances at 0.66 and 0.47 μm $\rho_{o0.66} / \rho_{o0.47}$ and the scattering angle Θ (Remer et al., 2005):

$$\eta = \frac{\left[\rho_{o0.66} / \rho_{o0.47} - 0.72\right]}{0.90 - 0.01(\Theta - 150°) - 0.72}$$

As an example, an AOT_F image on 5 August 2003 is depicted in figure 3.1.

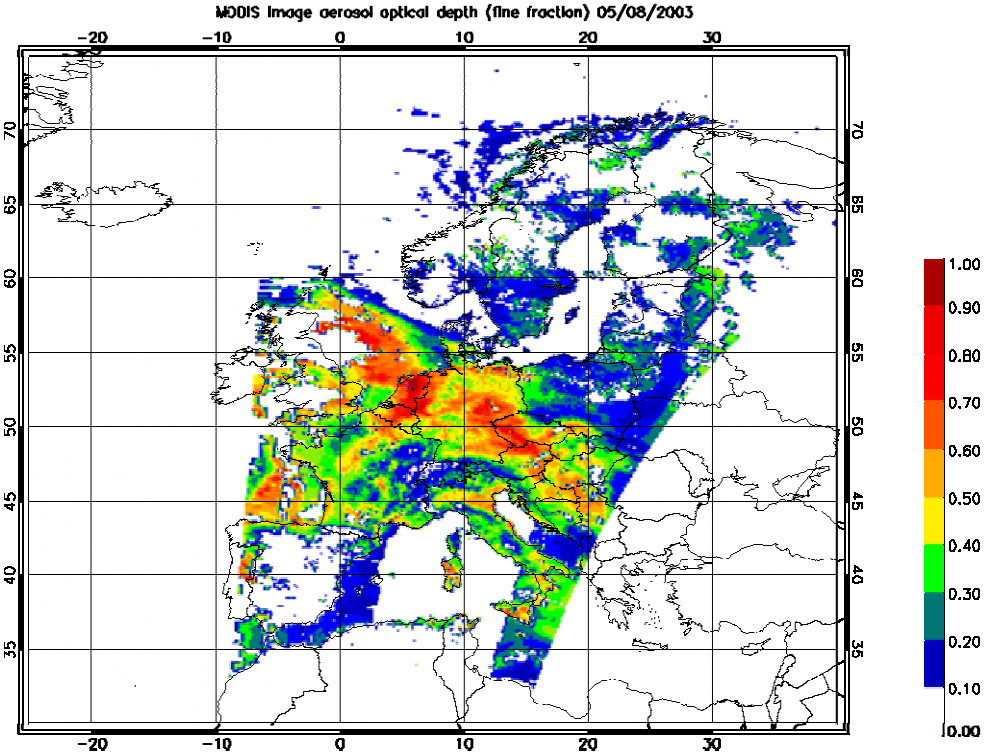

Figure 3.1 MODIS aerosol optical thickness (fine fraction) measured by the Terra satellite on 5 August 2003. Simulations with a chemistry-transport model for this day show that the high aerosol loading over the Netherlands and the North-Sea is caused by forest-fires in Portugal, which are advected over the Atlantic and the UK at an altitude of 3-4 km (Hodzic et al., 2005).

In this study, also the meteo-scaled optical thicknesses from the AOT and AOT were calculated. These are designated by AOT* and AOT_F*, respectively. Data of the boundary layer height and relative humidity at the surface were obtained from the ECMWF data archive. The three-hourly ECMWF data were interpolated in time and space to coincide with the MODIS overpass time.

3.2 Particulate matter concentrations from AirBase

Since the adoption of the EU air quality directives for particulate matter (EU, 1996; 1999), mass concentration measurements in Europe are performed operationally for particles smaller than 10 µm in diameter (PM_{10}). In the past few years, also more and more measurement sites are emerging for particles smaller than 2.5 µm in diameter ($PM_{2.5}$), as these are suspected to be more relevant for public health and therefore new air quality standards for $PM_{2.5}$ have been proposed by the European Commission to complement the PM_{10} standards.

These PM data are submitted to the AirBase data of the European Topic Centre on Air and Climate Change (ETC-ACC) of the European Environment Agency (EEA). This database consists of hourly or daily averaged values of PM, and meta-data, such as the latitude and longitude coordinates of the station, altitude, and information on its surroundings (urban background, (sub)urban background, street, industrial), measurement technique, etc.

Measurement techniques

The EU reference method to measure PM_{10} concentrations is described in CEN standard EN 12341, adopted by CEN in November 1998 (EN 12341, 1998). It defines a PM_{10} sampling inlet coupled with a filter substrate and a regulated flow device. The mass collected on the filter is determined gravimetrically by means of a microbalance under well-defined environmental conditions. This is the reference method under the First Daughter Directive; it gives, by definition, the 'correct' PM_{10} results.

However, for practical reasons (requirement of technique to be fully automatic), also other methods can be used if a Member State can demonstrate that it gives equivalent results or displays a consistent relationship to the reference method. In the latter case, results have to be corrected by a correction factor to produce results equivalent to the reference method. These correction factors can vary substantially in space and even seasonally. Differences between correction factors and the application itself hinder integration on a European scale of all PM_{10} data. An overview of correction factors used for PM_{10} data of 2002 in the AirBase database is given in Buijsman and de Leeuw (2004).

No European Reference Method for the measurement of the $PM_{2.5}$ fraction has been established up to now. Such a standard is currently being developed by CEN (CEN TC 264/Working Group 15) under a mandate of the European Commission. As for PM_{10}, the method is based on the gravimetric determination of the $PM_{2.5}$ fraction of particles in the air, sampled at ambient conditions. Also, for $PM_{2.5}$ fully automatic techniques are used. At present, no overview of applied correction factors for $PM_{2.5}$ exists.

At this moment, the most commonly used techniques for measuring PM are gravimetry (i.e., the reference method), the beta-absorption technique and the Tapered Element Oscillating Microbalance (TEOM) technique.

- The gravimetry method is based on directly weighing the collected aerosols. Ambient air is pumped with a constant flow rate into a specially shaped inlet where particulate matter is separated into size fractions. The particulate matter is then collected on a filter and weighed in a temperature and humidity controlled environment.
- With the beta-absorption technique the amount of particles on the filter is determined by measuring the attenuation of a beam of beta-radiation (electrons) which are send through the filter. The attenuation is proportional to the mass of the aerosols on the filter.
- The TEOM makes use of the change in eigen-frequency of a tapered glass element that is connected to the filter. The change in eigen-frequency is determined by the mass of particles attached to the filter.

Measurement of PM mass concentrations are subject to considerable uncertainties mainly because of alterations of the air sample during the measurement process. Alteration of the air sample highly depends on the environmental conditions and composition of the particles. Loss of semi-volatile particles is the major problem. In most cases the results from beta-absorption instruments as well as the TEOM underestimate the concentration (e.g. Hitzenberger et al., 2004; Charron et al., 2004). The comparability of the PM mass measurements of these samplers has therefore been recognized as a major issue of concern (CAFE-WGPM, 2004).

Measurement locations

The PM measurement stations are located in different surroundings. Most stations are representative for background conditions in rural, sub-urban and urban areas. These are typically representative for areas of several km^2 or larger. Also, there are many 'Traffic' stations, representative of concentration levels in streets and hence for a more limited area (scale of several tens of meters). A map of stations is presented in Figure 3.2.

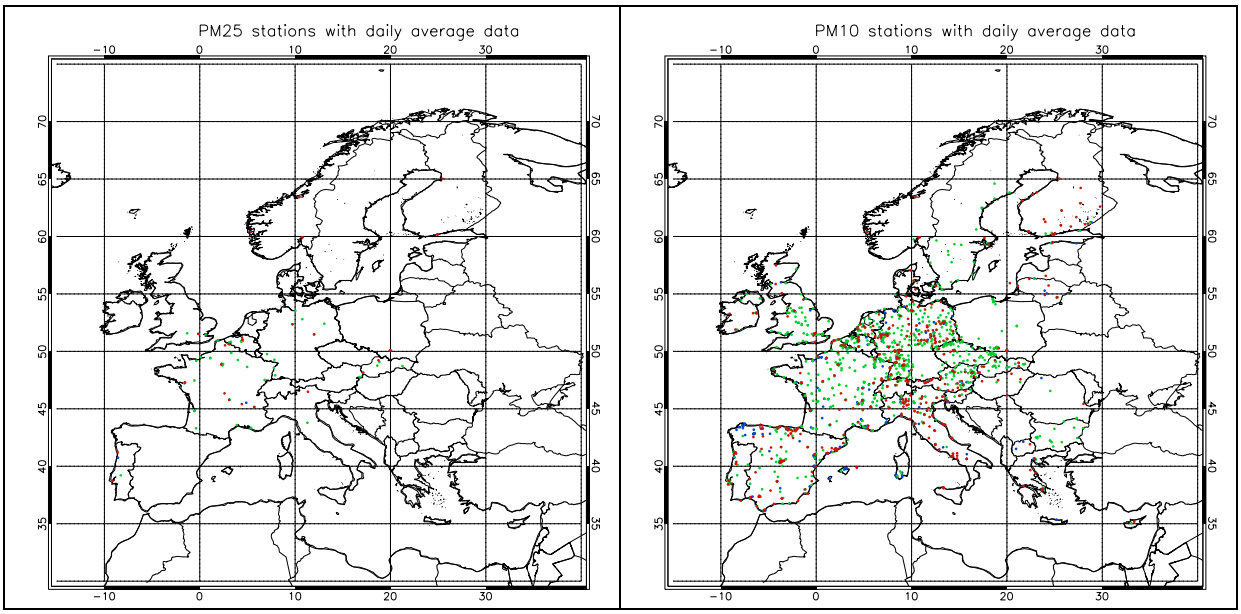

Figure 3.2 Map of AirBase stations with daily average data of $PM_{2.5}$ (left) and PM_{10} (right) in 2003. Red: Traffic stations; Green: Background stations; Blue: Other, which include industrial stations, and stations for which the surroundings are not reported.

In 2003, 28 European countries submitted their PM_{10} data and 11 countries their $PM_{2.5}$ data to AirBase, see Table 3.1. Most stations only deliver daily averaged PM concentrations to Airbase. From the 88 $PM_{2.5}$ stations that delivered daily average data, 23 stations also delivered hourly data. The meta-information in AirBase includes a description of the surroundings (rural, suburban of urban), the type of station (traffic, background, or other), the measurement method used, the altitude etc. In Table 3.1 also a division into the two main types of stations, namely traffic and background is presented.

A number of elementary quality checks have been done on the AirBase data, such as removing data from stations with clearly erroneous latitude/longitude coordinates.

Table 3.1 Number of PM_{10} and $PM_{2.5}$ measurement stations per country.

	PM10				PM2.5			
Country	**Total**	**Background**	**Traffic**	**Other/Unknown**	**Total**	**Background**	**Traffic**	**Other/Unknown**
Austria	95	50	34	11	1	1	0	0
Belgium	33	21	7	5	10	8	2	0
Bulgaria	14	14	0	0	0	0	0	0
Switzerland	22	14	7	1	0	0	0	0
Cyprus	2	1	1	0	0	0	0	0
Czech Republic	65	53	10	2	0	0	0	0
Germany	367	232	101	34	10	8	2	0
Denmark	8	4	4	0	0	0	0	0
Estonia	4	1	1	2	0	0	0	0
Spain	224	54	101	69	0	0	0	0
Finland	33	8	24	1	4	1	3	0
France	317	210	49	58	39	27	10	2
Great Britain	72	57	11	4	4	3	1	0
Greece	17	4	9	4	0	0	0	0
Hungary	8	3	5	0	0	0	0	0
Ireland	10	4	6	0	0	0	0	0
Italy	139	39	77	23	2	1	1	0
Lithuania	12	2	7	3	0	0	0	0
Latvia	1	0	1	0	0	0	0	0
Macedonia	3	0	1	2	0	0	0	0
Netherlands	33	22	11	0	0	0	0	0
Norway	7	2	5	0	4	0	4	0
Poland	32	27	2	3	3	1	1	1
Portugal	34	19	14	1	5	2	2	1
Romania	6	4	1	1	0	0	0	0
Sweden	25	21	4	0	0	0	0	0
Slovenia	7	4	3	0	0	0	0	0
Slovakia	26	19	6	1	6	4	2	0
Total	**1616**	**889**	**502**	**225**	**88**	**56**	**28**	**4**

In Table 3.2, an overview is given of measurement methods used for PM_{10} and $PM_{2.5}$. Clearly, most $PM_{2.5}$ measurements are performed with the TEOM, whereas most PM_{10} measurements are performed with the beta-absorption technique.

Table 3.2 Measurement method and station type of the measurement locations.

	PM2.5	PM10
Measurement method		
Oscillating Microbalance	57	484
Gravimetry	15	284
Beta-absorption	12	604
Other/Unknown	4	244
Stationtype		
(Sub-)urban background	40	650
Rural background	8	187
Traffic	28	502
Other	12	277

4. Data assimilation system of LOTOS-EUROS

In this chapter, an overview is given of the LOTOS-EUROS model (Section 4.1) and the data-assimilation system (Section 4.2).

4.1 Modelling PM and AOT in LOTOS-EUROS

Domain
The master domain of LOTOS-EUROS is bound at 35° and 70° North and 10° West and 60° East. The projection is normal longitude-latitude and the standard grid resolution is 0.50° longitude x 0.25° latitude, approximately 25x25 km^2. In this study, several domains within this master domain were considered. The final results are calculated over a domain that covers Europe (up to 40° East) but excludes the largest part of European Russia. In the vertical there are three dynamic layers and an optional surface layer. The model extends in vertical direction 3.5 km above sea level. The lowest dynamic layer is the mixing layer, followed by two reservoir layers. The height of the mixing layer is part of the diagnostic meteorological input data. The heights of the reservoir layers are determined by the difference between the mixing layer height and 3.5 km. Both reservoir layers are equally thick with a minimum of 50m. In some cases when the mixing layer extends near or above 3500 m the top of the model exceeds the 3500 m according to the abovementioned description. Simulations were performed with the optional surface layer of a fixed thickness of 25 m. Hence, this layer is always part of the dynamic mixing layer. For output purposes the concentrations at measuring height (usually 3.6 m) are diagnosed by assuming that the flux is constant with height and equal to the deposition velocity times the concentration at height z.

Transport
The transport consists of advection in 3 dimensions, horizontal and vertical diffusion, and entrainment/detrainment. The advection is driven by meteorological fields (u,v) which are input every 3 hours. The vertical wind speed w is calculated by the model as a result of the divergence of the horizontal wind fields. The recently improved and highly-accurate, monotonic advection scheme developed by Walcek (2000) is used to solve the system. The number of steps within the advection scheme is chosen such that the courant restriction is fulfilled. Entrainment is caused by the growth of the mixing layer during the day. Each hour the vertical structure of the model is adjusted to the new mixing layer thickness. After the new structure is set the pollutant concentrations are redistributed using linear interpolation. The horizontal diffusion is described with a horizontal eddy diffusion coefficient following the approach by Liu and Durran (1977). Vertical diffusion is described using the standard Kz-theory. Vertical exchange is calculated employing the new integral scheme by Yamartino et al. (2004).

Chemistry
The LOTOS-EUROS model contains two chemical mechanisms, the TNO CBM-IV scheme (Schaap et al., 2005a) and the CBM-IV by Adelman (1999). In this study, the TNO CBM-IV scheme is used, which is a modified version of the original CBM-IV (Whitten et al., 1980). The scheme includes 28 species and 66 reactions, including 12 photolytic reactions. Compared to the original scheme steady state approximations were used to reduce the number of reactions. In addition, reaction rates have been updated regularly. The mechanism

was tested against the results of an intercomparison presented by Poppe et al. (1996) and found to be in good agreement with the results presented for the other mechanisms. Aerosol chemistry is represented using ISORROPIA (Nenes et al., 1999).

Dry and wet deposition

The dry deposition in LOTOS-EUROS is parameterised following the well known resistance approach. The deposition velocity is described as the reciprocal sum of three resistances: the aerodynamic resistance, the laminar layer resistance and the surface resistance. The aerodynamic resistance is dependent on atmospheric stability. The relevant stability parameters (u*, L and K_z) are calculated using standard similarity theory profiles. The laminar layer resistance and the surface resistances for acidifying components and particles are described following the EDACS system (Erisman et al., 1994).

Below cloud scavenging is described using simple scavenging coefficients for gases (Schaap et al., 2004) and following Simpson et al. (2003) for particles. In-cloud scavenging is neglected due to the limited information on clouds. Neglecting in-cloud scavenging results in too low wet deposition fluxes but has a very limited influence on ground level concentrations (see Schaap et al., 2004).

Meteorological input

The LOTOS-EUROS system is presently driven by 3-hourly meteorological data. These include 3D fields for wind direction, wind speed, temperature, humidity and density, substantiated by 2-dimensional gridded fields of mixing layer height, precipitation rates, cloud cover and several boundary layer and surface variables. The standard meteorological data for Europe are produced at the Free University of Berlin employing a diagnostic meteorological analysis system based on an optimum interpolation procedure on isentropic surfaces. The system utilizes all available synoptic surface and upper air data (Kerschbaumer and Reimer, 2003). Also, meteorological data obtained from ECMWF can be used to force the model.

Emissions

The anthropogenic emissions used in this study are a combination of the TNO emission database (Visschedijk et al., 2005) and the CAFE baseline emissions for 2000. For each source category and each country, the country totals of the TNO emission database were scaled to those of the CAFE baseline emissions. Elemental carbon (EC) emissions were derived from (and subtracted from) the primary $PM_{2.5}$ ($PPM_{2.5}$) emissions following Schaap et al. (2004b). Hence, the official emission totals were used as used within the LRTAP protocol, but also the benefit are exploited from the higher resolution of the TNO emission database (0.25x0.125 lon-lat). The annual emission totals are broken down to hourly emission estimates using time factors for the emissions strength variation over the months, days of the week and the hours of the day (Builtjes et al., 2003).

In LOTOS-EUROS biogenic isoprene emissions are calculated following Veldt (1991) using the actual meteorological data. In addition, sea salt emissions are parameterised following Monahan et al (1986) from the wind speed at ten meter height. Dust was neglected as it normally does not contribute a large fraction to the fine aerosol mass in Europe and, more importantly, because there are no reliable emission estimates and/or parameterisations

Boundary conditions

The boundary conditions for ozone are derived from the 3-dimensional tropospheric ozone climatology by Logan (1998), which is derived from ozone sonde data. For a number of components, listed in Table 4.1 the EMEP method is followed (Simpson et al., 2003) based on measured data. In this method simple functions have been derived to match the observed distributions. The boundary conditions are adjusted as function of height, latitude and day of the year. The functions are used to set the boundary conditions, both at the lateral boundaries as at the model top. The annual cycle of each species is represented with a cosine-curve, using the annual mean near-surface concentration, C_0, the amplitude of the cycle ΔC, and the day of the year at which the maximum value occurs, d_{max}. Table 4.1 lists these parameters.

First the seasonal changes in ground-level boundary condition, C_0, are calculated through:

$$C_0 = C_{mean} + \Delta C \cdot \cos\left(2\pi \frac{(d_{mm} - d_{\max})}{n_y}\right)$$

where n_y is the number of days per year, d_{mm} is the day number of mid-month (assumed to be the 15th), and d_{max} is day number at which C_0 maximizes, as given in Table 4.1. Changes in the vertical are specified with a scale-height, H_z, also given in Table 4.1.

$$C_i(h) = C_0 e^{-\frac{h}{Hz}}$$

where $C_i(h)$ is the concentration at height h (in km). For simplicity h is set to be the height of the centre of each model layer assuming a standard atmosphere. For some species a latitude factor, given in Table 4.2, is also applied. Values of C_i adjusted in this manner are constrained to be greater or equal to the minimum values, C_{min}, given in Table 4.1. Ammonia boundary conditions are neglected. Sulphate is assumed to be fully neutralized by ammonium. Nitrate values are assumed to be included in those of nitric acid and are zero as well.

Table 4.1 Parameters used to set the boundary conditions

Parameter	C_{mean}	d_{max}	ΔC	H_z	$C_0^{\min}$	$C_h^{\min}$
	ppb	days	ppb	km	ppb	ppb
SO_2	0.15	15.0	0.05	∞	0.15	0.03
SO_4	0.15	180.0	0.00	1.6	0.05	0.03
NO	0.1	15.0	0.03	4.0	0.03	0.02
NO_2	0.1	15.0	0.03	4.0	0.05	0.04
PAN	0.20	120.0	0.15	∞	0.20	0.1
HNO_3	0.1	15.0	0.03	∞	0.05	0.05
CO	125.0	75.0	35.0	25.0	70.0	30.0
ETH	2.0	75.0	1.0	10.0	0.05	0.05
FORM	0.7	180.0	0.3	6.0	0.05	0.05
ACET	2.0	180.0	0.5	6.0	0.05	0.05

Table 4.2 Latitude factors applied to the prescribed boundary conditions

Component	Latitude (°N)							
	35	40	45	50	55	60	65	70
SO_2, SO_4, NO, NO_2	0.15	0.3	0.8	1.0	0.6	0.2	0.12	0.05
HNO3, FORM, ACET	1.0	1.0	0.85	0.7	0.55	0.4	0.3	0.2
PAN	0.33	0.5	0.8	1.0	0.75	0.5	0.3	0.1
CO	0.7	0.8	0.9	1.0	1.0	0.95	0.85	0.8

AOT calculation

The AOT is computed from the dry aerosol mass concentrations derived from the LOTOS-EUROS model using the approach of Kiehl and Briegleb (1993):

$$AOT_i(\lambda) = f(RH, \lambda) * a_i(\lambda) * B_i(\lambda)$$

where $a_i(\lambda)$ is the mass extinction efficiency of the compound i; B_i is the column burden of the compound i; f (RH, λ) is a function describing the variation of the scattering coefficient with relative humidity (RH) and wavelength (l). To compute $a_i(\lambda)$ for dry inorganic particles, a Mie (Mie, 1908) code has been used, assuming the aerosol size distribution to be log-normal, with a geometric mean radius of 0.05μm, a geometric standard deviation of 2.0 and a sulphate dry particle density of 1.7 g cm^{-3} (Kiehl and Briegleb, 1993). Most aerosol particles absorb or release water vapour when the relative humidity (RH) changes. Thus the size and composition of the particles change, resulting in different light scattering properties. To account for the variation of the aerosol scattering coefficient with RH, the factor f(RH, λ), derived from humidity controlled nephelometry (Veefkind et al., 1996), is used (see Figure 2.2). Similar functions for f(RH) have been reported by Day et al. (2001) for various locations in the United States. Effects due to hysteresis (e.g. Tang, 1997) are not accounted for. The wavelength dependence of f (RH) can be ignored (Veefkind et al., 1999). The scattering calculations were made with RH values taken from the analysed meteorological data file that is used as input to the LOTOS-EUROS model, including the variations of RH with height. For the organic aerosol components an a_i of 9 for EC and 7 for OC is assumed (Tegen et al., 1997). For these components the growth as function of RH has been neglected.

4.2 Ensemble Kalman filter

The first step in order to build the Ensemble Kalman Filter around LOTOS-EUROS is to embed the model and the available measurement in a stochastic environment:

$$x^{k+1} = f^k(x^k, w^k)$$
$$y^k = C^k x^k + v^k,$$

where the superscripts (k) denote the time-steps. The model state vector is denoted by *x* and the measurements by *y*. The function *f* denotes the non-linear model operator which apart from on the state vector acts on a white noise vector *w* with Gaussian distribution and diagonal covariance matrix *Q*. The measurement vector *y* is assumed be a linear combination of elements of the state vector and a random, uncorrelated Gaussian error *v* with (diagonal) covariance matrix *R*. The basic idea behind the ensemble filter is to express the probability function of the state in an ensemble of possible states $\{\xi_1, ..., \xi_N\}$, and to approximate statistical moments with sample statistics:

$$\hat{x} \approx \frac{1}{N}\sum_{j=1}^{N}\xi_j$$

$$P \approx \frac{1}{N-1}\sum_{j=1}^{N}\left(\xi_j - \hat{x}\right)\left(\xi_j - \hat{x}\right)^T$$

where the pair ($\hat{x}$,*P*) (expectation and covariance matrix) describe the probability of the state vector *x* completely if *x* has a Gaussian distribution. Since the models are strongly non-linear, it cannot be expected that *x* really has a Gaussian distribution. It is assumed however that the distribution is at least close to Gaussian so that the bulk of the statistical properties is captured by the pair ($\hat{x}$,*P*). The filter algorithm consists of three stages:

initialisation:
each ensemble member is set to the initial state:

$$\xi_j = x^0$$

forecast:
each ensemble member is propagated in time by the model, where the noise input w^k is drawn from a random generator with covariance Q;

$$\xi_j^f = f(\xi_j, w^k)$$

analysis:
given an (arbitrary) gain matrix K, each ensemble member is updated according to:

$$\xi_j^a = \xi_j^f + K(y + \nu - H^T\xi_j^f)$$

where ν represents a measurement error, drawn from a random generator with zero mean and covariance *R*. The gain matrix *K* is given by the optimal gain matrix from the original Kalman Filter. In the original filter the Kalman gain was obtained by matrix multiplications in which the covariance matrix *P* is involved. Fortunately, the use of this matrix can be avoided, since this matrix is too large to store into memory. Instead, a square root *S* (such that $P=SS^T$) can be used. From the definition of *P* it can be seen that the columns s_i of such a square root can be defined by

$$s_i = \frac{1}{\sqrt{N-1}}\left(\xi_i - \hat{x}\right)$$

.

Note that the sample mean $\hat{x}$, and the matrix *S* completely define the ensemble and vice versa; it is therefore not necessary to store both *S* and the ensemble. The analysis of the measurements y_j (entries of the vector *y*) can now be performed by the following sequential procedure (dropping the time index):

$$h_j = S_{j-1}^T c_j^T$$
$$a_j = \left(h_j^T h_j + r_{jj}\right)^{-1}$$
$$b_j = \left(1 + \sqrt{a_j r_{jj}}\right)^{-1}$$
$$k_j = a_j S_{j-1} h_j$$
$$S_j = S_{j-1} - b_j k_j h_j^T$$
$$x_j = x_{j-1} + h_j \left(y_j - c_j x_{j-1}\right)$$

The index *j* is the iteration index. The starting values for the procedure are $S_0 = S_f^{k+1}$ and $x_0 = x_f^{k+1}$. After the analysis of all the measurements the final values for the state vector and (square root of) the covariance matrix have been obtained: $S^{k+1} = S_m$ and $x^{k+1} = x_m$. For a detailed description, reference is made to Van Loon et al. (2000) and Evensen (1997).

The forecast step is the most expensive part of the algorithm, since for each ensemble member the model has to be evaluated one time. Typical ensemble sizes range from 10-100. If the number of measurements is limited (in order of hundreds), the total computation time involved with the ensemble filter is proportional with the ensemble size.

Random noise

In the model implementation used in this study, the noise parameters are part of the model state. Hence they are estimated by the filter as well. In Chapter 7, the noise to several emission fields E_j is specified. The noise parameters w_i can be interpreted as emission correction factors since the actual emission field E_j is estimated by the filter as

$$E_i \leftarrow E_j\ (1+w_i).$$

This approach has the disadvantage that there is no 'memory' in the system: the w_i are uncorrelated in time; at a certain hour *t* the noise parameter may indicate an emission increase of 20% with respect to the original field, whereas it estimates a decrease of 20% at *t+1*. Such irregular behaviour can be prevented to a large extent by the use of coloured noise. However, in the present set-up, the same noise factors for the 24 hour period between overpasses were used. Hence, the long period between the measurements warrants some correlation in time.

Spatially limiting influence of measurements

For two reasons correlations between elements in the state vector arise which are unlikely to be correlated. Firstly, spurious correlations arise, mainly because the sample size is finite. Secondly, undesired correlations arise due to the choice of the noise processes. The noise processes to be introduced in this study are all acting on emission fields of various emitted compounds causing 'instantaneous' correlations throughout the domain. For example the particulate matter concentration at hour *t* somewhere in The Netherlands becomes correlated with the particulate matter concentration in, say, the south of France, because noise was added to the NO_x emission field at hour *t*-1. Although this is exactly what should happen when defining noise in this way, such correlations are not realistic and should be somehow ignored by the filter. The noise processes is chosen this way because it is infeasible to subdivide the emission fields into a number of sub-domains on each of which a different noise parameter is acting. That would increase the dimension of the noise vector dramatically and hence the necessary ensemble size to capture the statistical properties.

One way to ignore unrealistic correlations over large distances is the use of a gain matrix which is only unequal to zero around the locations of observations. Such a gain matrix k may be formed using a covariance matrix which is an element wise product of the original sample covariance and a correlation function with local support. For a single scalar measurement, the resulting gain matrix is given by (omitting the subscripts):

$$k = I(\rho)Ph/(h^T Ph + r)$$

where $I(\rho)$ is a diagonal matrix; the diagonal elements are filled with a prescribed correlation between the corresponding grid cell and the grid cell of the measurement. Different choices for the values of ρ_i are possible. In this study it is assumed that

$$\rho_i = \exp(-0.5\ (r_i/L)^2) \quad \text{for } r_i \leq 3.5\ L$$

and zero otherwise. r_i denotes the distance from the grid cell considered to the site of the analysed measurement and L denotes a length scale parameter, taken to be 100 km in this study.

5. Validation of MODIS AOT using AERONET

5.1 Analysis of yearly average data

AERONET is an optical ground based aerosol monitoring network supported by NASA's Earth Observing System and other international institutions. It consists of identical automatic sun-sky scanning spectral radiometers. The network provides, among others, globally distributed observations of aerosol optical thickness. In previous studies, the retrieved AOT has been validated against a limited set of AOT measurements from the ground-based AERONET network on a global scale. These validations showed that the retrieved AOT is generally within the pre-specified accuracy of ±0.05±0.20AOT over land and ±0.03±0.05AOT over oceans (1-σ level, for individual retrievals), except in situations with possible cloud contamination, over surfaces with sub pixel surface water such as coastal areas and over surfaces with sub pixel snow cover (Chu et al., 2002; Ichoku et al., 2005). In this study, MODIS AOT and AOT_F were validated against AERONET observations of in more detail for Europe in 2003.

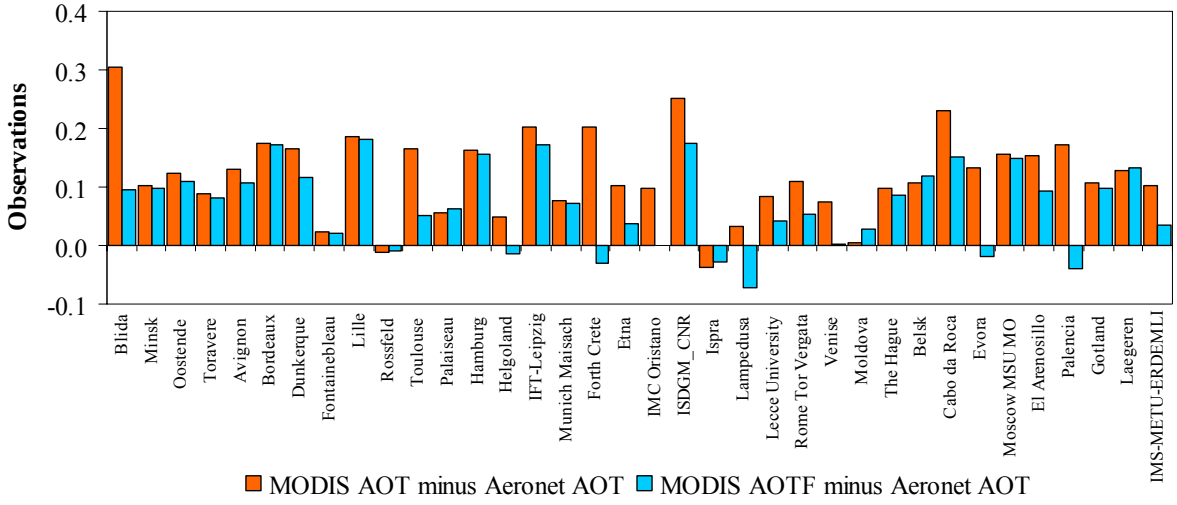

Figure 5.1 Difference between AERONET AOT and MODIS AOT (and AOT_F) at AERONET stations.

For our validation exercise all 36 AERONET stations that provided data for 2003 in Europe were used. Figure 5.1 shows the difference in the absolute values of MODIS and AERONET AOT for the individual stations. It is evident from Figure 5.1 and Table A.1 (Annex 1) that MODIS generally overestimates the AOT values measured by AERONET at almost all the stations. The difference is variable for the different stations. On average, the annual mean AOT and AOT_F observed by MODIS across all stations are 0.30 and 0.25 respectively, while that observed at AERONET stations is 0.20, providing a mean annual difference of 0.10 for AOT and 0.05 for AOT_F across all stations. For western Europe, the extent of the overestimation by MODIS is in agreement with findings from Remer et al. (2005).

Besides average differences, also the spatial correlation of yearly average optical thicknesses were considered. This is particularly important, as the spatial gradients of yearly average AOT play an important role if the AOT is used for improvement of mapping yearly average PM levels. It was found that the spatial correlation between AERONET AOT and MODIS is 0.64 for the AOT and 0.72 for the AOT_F.

5.2 Analysis of time-series per station

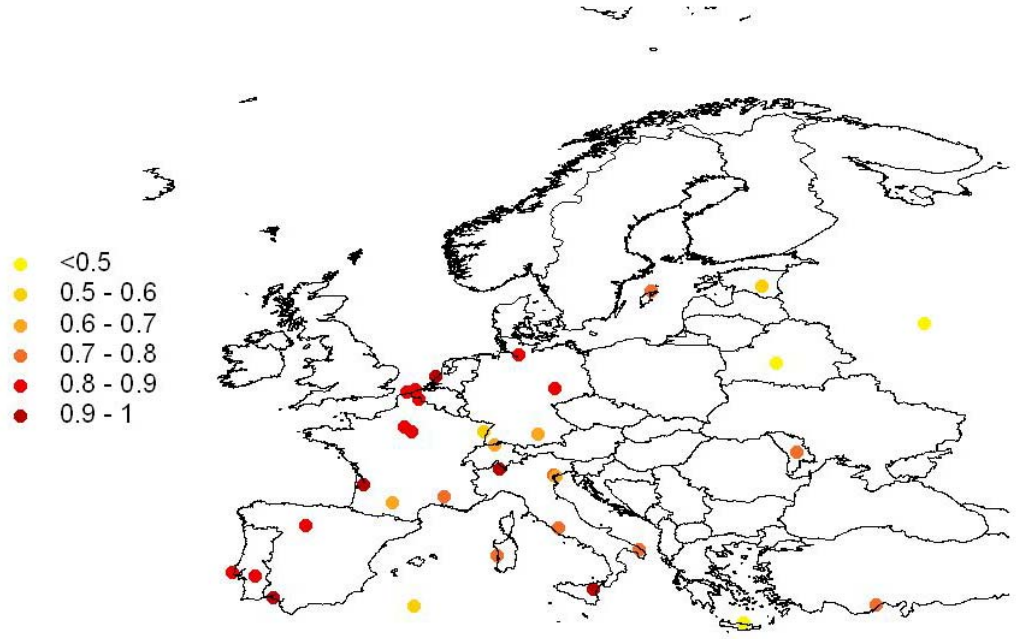

Figure 5.2 Time correlations between AOT from AERONET and MODIS.

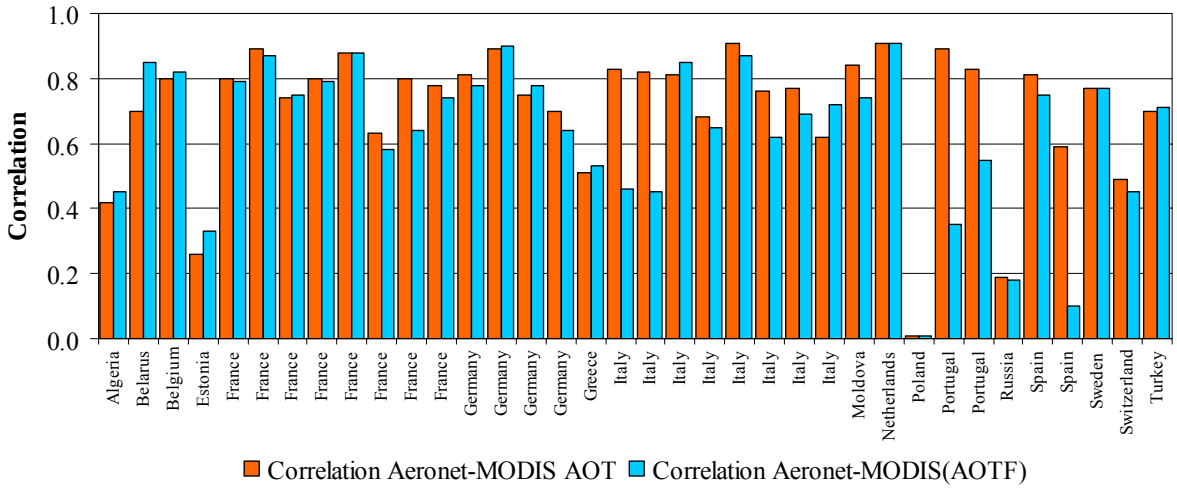

Figure 5.3 Time correlations between AERONET AOT and MODIS AOT (AOT_F).

The temporal correlations between the MODIS and AERONET at the AEORNET stations are presented in Figures 5.2 and 5.3 and are also listed in Table A.1 (Annex 1). The time-series of MODIS and AERONET AOT show a correlation of 0.72, averaged over all stations. The median of the correlation coefficients is 0.77. For MODIS AOT_F versus AERONET AOT, these correlations are slightly lower. This is understandable, since the AOT_F only pertains to the optical thickness due to the smaller particles. Indeed, particularly in Southern Europe, (southern Italy, Portugal and Spain), the correlations with AOT_F are sometimes much lower

than those with the AOT. This might point at a high contribution of coarse particles to the AOT. This is consistent with the fact that the difference between yearly average AOT and AOT_F observed by MODIS is large at these stations. Poor correlation coefficients are found for stations with sparse data (e.g, Belsk, Poland). Stations with less than 15 days with simultaneous measurements have therefore been removed from the analysis.

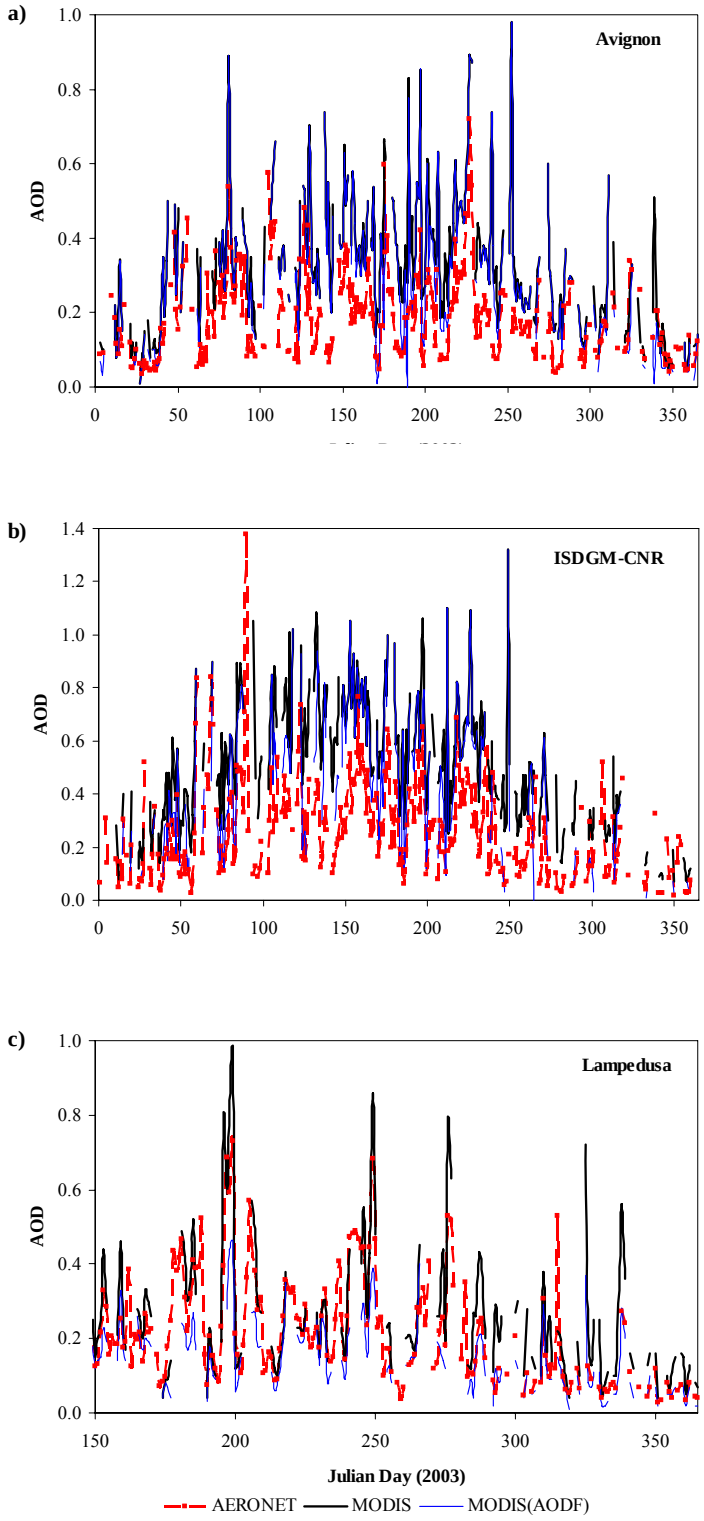

Figure 5.4 Temporal variation of AERONET AOT and MODIS AOT and AOT_F at a) Avignon (France), b) ISDGM-CNR (Italy), and c) Lampedusa (Italy).

In general, MODIS AOT and AOT_F exhibit a similar seasonal variation to that observed at AERONET stations. Examples are given in Figure 5.4 for Avignon (France), ISDGM-CMR (Italy), and Lampedusa (Italy, in the Mediterranean sea) . Generally high AOT (AOT_F) values are being observed in summer and low AOT (AOT_F) values in winter. The MODIS AOT, however, exhibits a stronger seasonal trend than AERONET AOT. The difference between MODIS and AERONET AOT and AOT_F is summarized for all sites in Figure 5.5. In winter and summer average residuals for AOT (AOT_F) are 0.05 (0.01) and 0.16 (0.10), respectively. In a relative sense, the difference remains practically constant throughout the year (see Figure 5.6). On the whole, the AERONET AOT is about 70% of MODIS AOT and 90% of MODIS AOT_F.

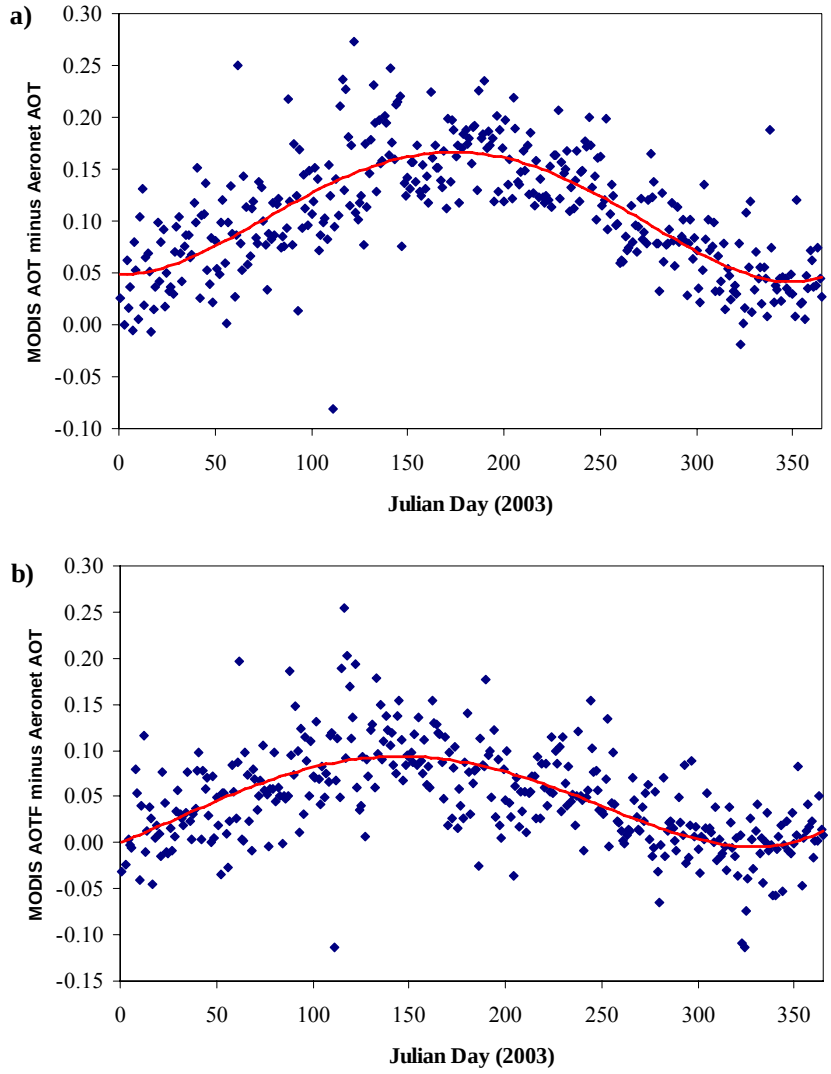

Figure 5.5 a) Seasonal variation of the absolute difference between MODIS and AERONET AOT for all sites averaged; b) Same as (a), but for the AOT_F from MODIS.

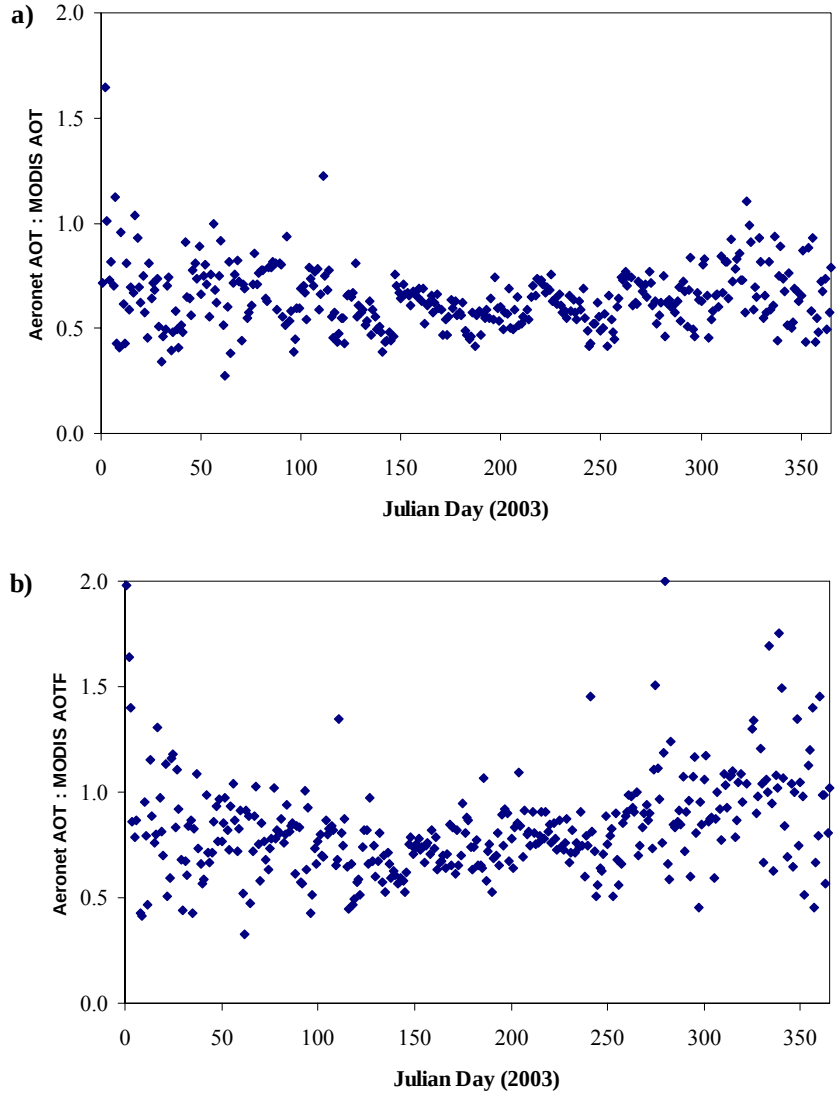

Figure 5.6 a) Relative difference between MODIS and AERONET AOT for all sites averaged, and b) Same as (a), but for the AOT_F from MODIS.

It was investigated whether the MODIS AOT is as accurate (1-sigma error ±0.05±0.20AOT) as claimed in the literature. Table 5.1 summarises the percentage of MODIS retrievals for which the AERONET observation is within 1 or 2 sigma from the MODIS retrieval. From a statistical point of view, and assuming normally distributed data, 66% of the data should be within the 1-sigma and 95% within the 2-sigma range. The MODIS AOT does not fulfil this requirement, which is attributed to the relatively high bias in these data. After correction for the bias (simply by multiplication AOT data with 0.7, and AOT_F data with 0.9), the MODIS accuracy agrees within 1-sigma limits ±0.05±0.20AOT. The frequency distributions of the bias-corrected difference between AERONET and MODIS are shown in Figure 5.7.

Table 5.1 Percentage of MODIS retrievals for which the AERONET observation is within 1 or 2 sigma from the MODIS retrieval, where sigma = ±0.05± 0.20AOT.

	% within 1-sigma	% within 2-sigma
AOT	55	91
AOT* 0.7	73	96
AOT_F	64	93
AOT_F * 0.9	68	93

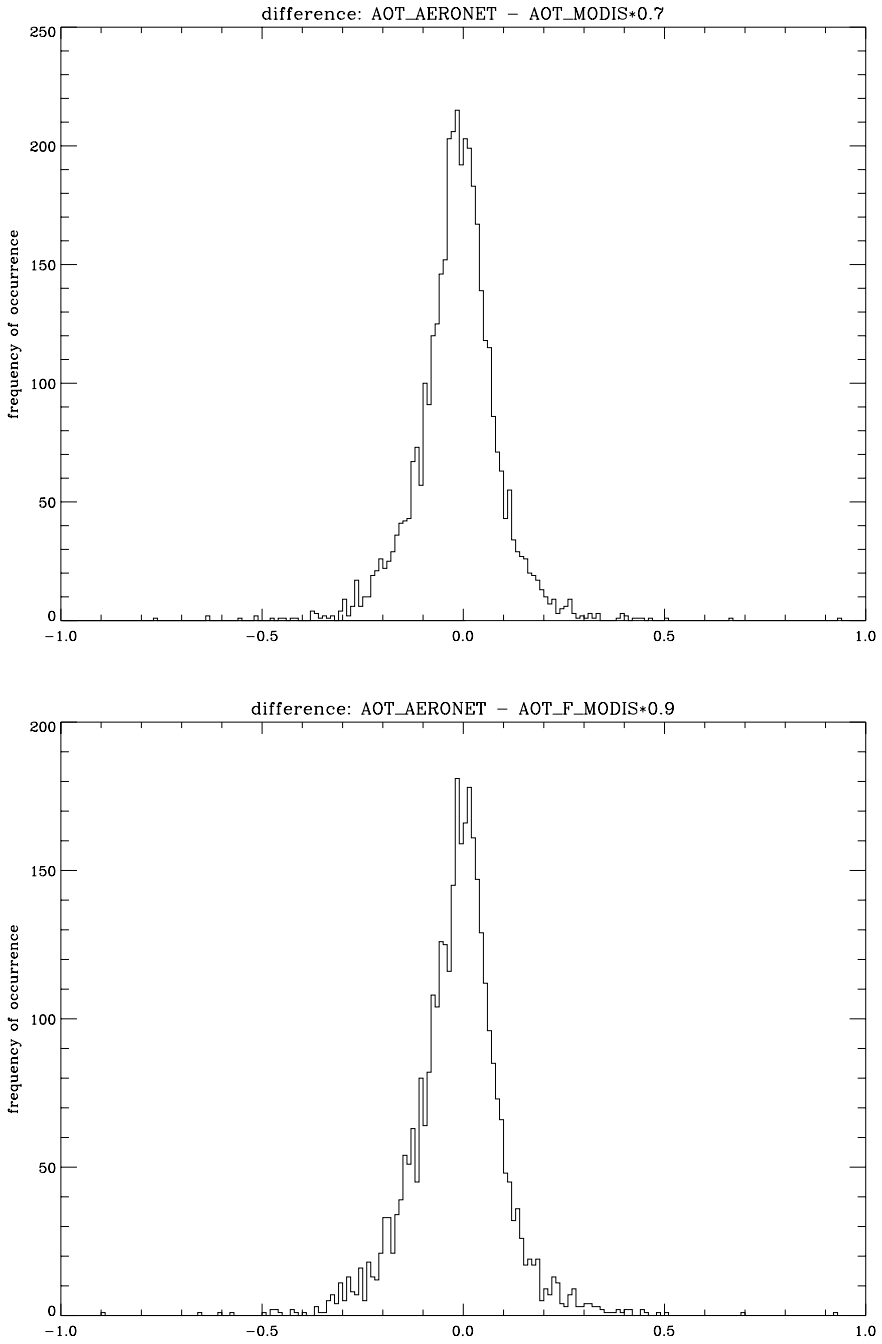

Figure 5.7 Frequency distributions of the difference between AERONET and MODIS (bias corrected). Top: AERONET versus MODIS AOT, Bottom AERONET versus MODIS AOT_F.

5.3 Conclusions of the validation

In this chapter, MODIS AOT and AOT_F have been validated against ground-based measurements made at various AERONET stations above Europe.

The spatial correlation between MODIS and AERONET observed yearly average AOT over Europe is 0.64 for AOT and 0.72 for AOT_F. However, the results show that MODIS systematically overestimates the AOT. On average, the annual mean AOT (AOT_F) observed by MODIS across all validation stations is 0.30 (0.25) compared to 0.20 as obtained by the AERONET sun-photometers. A more or less constant factor was found between MODIS AOT and AOT_F and AERONET, of 0.7 and 0.9, respectively. After correction of the AOT_F values, through multiplication with 0.9, the both the AOT and the AOT_F data agree with AERONET within an uncertainty range of $\pm 0.05 \pm 0.2 AOT_F$.

The temporal correlation between MODIS and AERONET observed AOT is generally high, with a mean correlation of 0.72 (0.77 median of all stations). For the AOT_F these temporal correlations are slightly lower, particularly in Southern-European stations, and this is likely to reflect frequent occurrence of coarse aerosols there.

Because of the higher spatial correlation of AOT_F with AERONET, the lower bias of AOT_F, and the spatial higher correlation of AOT_F with $PM_{2.5}$ (see Section 6.1), the AOT_F was used for the assimilation and statistical mapping of $PM_{2.5}$, rather than the AOT itself.

6. Mapping of $PM_{2.5}$ – statistical approach

In this chapter, results are presented of the multiple regression approach to map $PM_{2.5}$ concentrations. Section 6.1 focuses on spatial distributions and spatial correlations of yearly average AOT and PM values (both PM_{10} and $PM_{2.5}$). In that section, the comparison is limited to rural background stations, because the primary interest there is to compare the large-scale spatial characteristics of AOT and PM across Europe. Section 6.2 describes temporal correlations between monthly and daily average AOT and PM time-series. For processing reasons, the comparison is limited to those stations that simultaneously measured both PM_{10} and $PM_{2.5}$. The results of the multiple regression approach are presented in Section 6.3.

6.1 Comparison of spatial distributions of yearly average AOT and PM

All MODIS AOT images over Europe (both Terra and Aqua; Collection 4 data) were acquired for the year 2003. Subsequently, the AOT data were binned into a 0.1° by 0.1° grid over Europe, and the average has been calculated for each month of the year. This grid size is approximately 10x5 km^2 in Europe, and was chosen to be of the same order of magnitude as the MODIS AOT itself.

Typically, in summer months, the monthly average is based on 15-20 AOT measurements that are available per grid cell. In winter months, typically 5-10 measurement points are available for averaging, and this is restricted to latitudes below about 50 N. For latitudes above 50 N, no data are available in mid-winter, because the solar elevation is too low at these latitudes to allow retrieval of AOT. Also in the Alps, and Central Europe several (winter) months are excluded because of too much snow cover in winter for the AOT retrieval, and no data are available over the Saharan desert, because the surface is too bright to allow AOT retrieval. Yearly average maps are calculated from the monthly average maps, using only those months for which a monthly average is available. Hence, 'yearly' averages for these regions above 50 N are in fact averages excluding one or more months around the shortest day in the year. Our analysis is based on both MODIS-Terra (morning) and MODIS-Aqua (afternoon) observations. It was found that the Aqua observations generally yield slightly higher AOT values than the Terra observations, as was also noted by Ichoku et al. (2005).

The yearly average AOT (at 0.55 μm) for Europe in 2003 is shown in figure 6.1. Areas in Europe with high AOT are found in the densely populated and industrialized areas throughout Europe (individual cities and clusters of cities) and large areas in Central Europe. Particularly high values are found for the Netherlands, Belgium, the Ruhr aera, the Po-valley, Northern Germany and the former East-Germany, Poland, and parts of Central European countries (particularly areas around the Danube river). Also smaller scale features can be distinguished, such as several major cities like Rome, Paris, and Athens; also the Rhone-valley is clearly distinguishable. Furthermore, high AOT values are also found for semi-arid rural areas in Southern Europe (particularly in Spain and Turkey). Low values are observed in Northern Europe and over mountain areas throughout Europe (Alps, Pyrenees, Masif Central, Carpates, etc.). Clearly, most aerosols are detected close to their source regions. In more detail, along coastal areas like The Netherlands, sometimes unrealistically high AOT

values are observed. At land/water boundaries, application of the land algorithm to patches of sea or ocean is likely to lead to too high AOT values (Chu et al., 2002). Also, a discontinuity in AOT can be observed near the 25° E meridian, which coincides with a different assumption on aerosol type in the MODIS algorithm. Apparently, this gives rise to a systematic bias in the AOT.

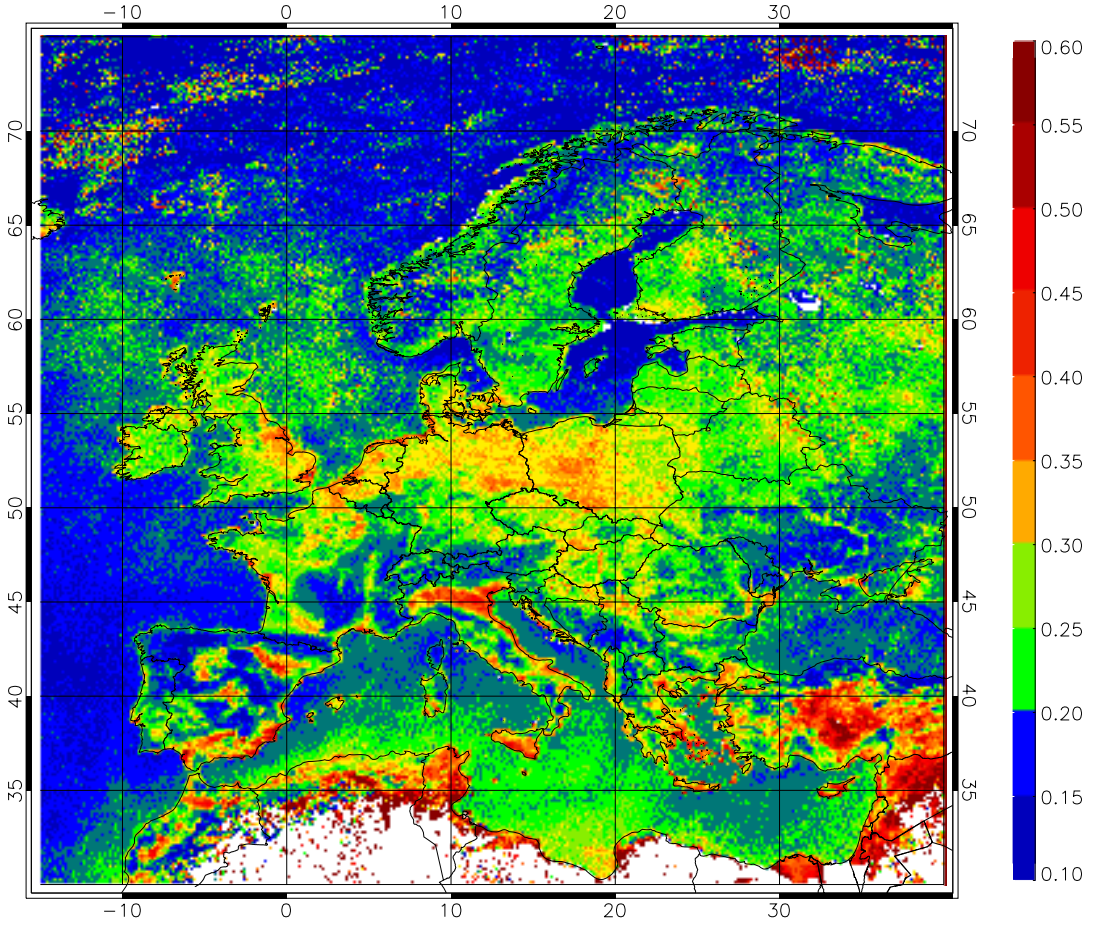

Figure 6.1 Yearly average aerosol optical thickness over Europe (at 0.55 µm) measured by MODIS in 2003. White: missing data.

The spatial distribution of the yearly average of the fine fraction of the AOT, AOT_F, generally resembles that of the AOT for Northern and Central Europe (see figure 6.2). In Southern Europe however, AOT_F values are often much lower than the AOT values, particularly in semi-arid areas in Spain, Italy and Turkey. These areas even show the lowest values of AOT_F in Europe, while they show high AOT values. A low ratio of AOT_F/AOT is not unlikely for such areas, because they can be a major source of coarse aerosol particles (Querol et al., 2004). Also, it is apparent that AOT_F values are generally much lower than the AOT for pixels with mixed land/water surfaces.

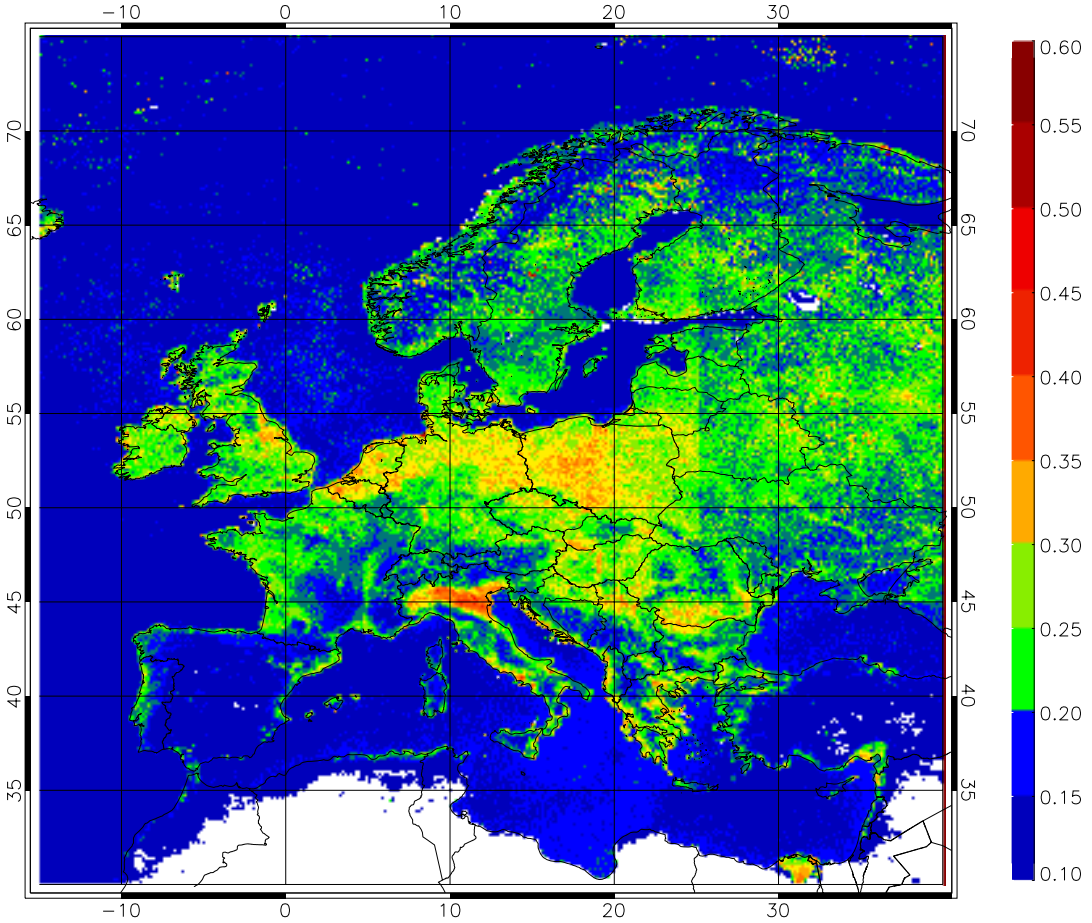

Figure 6.2 Same as figure 6.1, but for the fine fraction of the aerosol optical thickness.

Figure 6.3 depicts the yearly average Ångström-parameter. The Ångström-parameter depends on the size of the aerosol particles, and is small for coarse particles and increases with decreasing particle size. It can be observed that, according to MODIS, the Ångström parameter is 1.5 or larger for most of the European continent, but is smaller in large parts of Spain, Sicily, and Turkey, and hence gives rise to a low AOT_F/AOT ratio. However, caution must be exercised because the Ångström-parameter is even more sensitive to the assumptions on the spectral dependence of the land surface than the AOT, and may be biased for specific surface types or seasons. The Ångström-parameter appears to be lower over the oceans than over land, but over land the Ångström-parameter is based on the 0.44 and 0.66 µm channels, while that over ocean is based on the 0.55 and 0.87 µm channels. This hampers a direct numeric comparison between land and ocean. Nevertheless, the Ångström-parameter over the southern part of the North Sea is relatively large (indicating relatively small particles) compared to other parts of the North Sea, which can be the result of shipping emissions, and transport of aerosols from continental Europe and the UK.

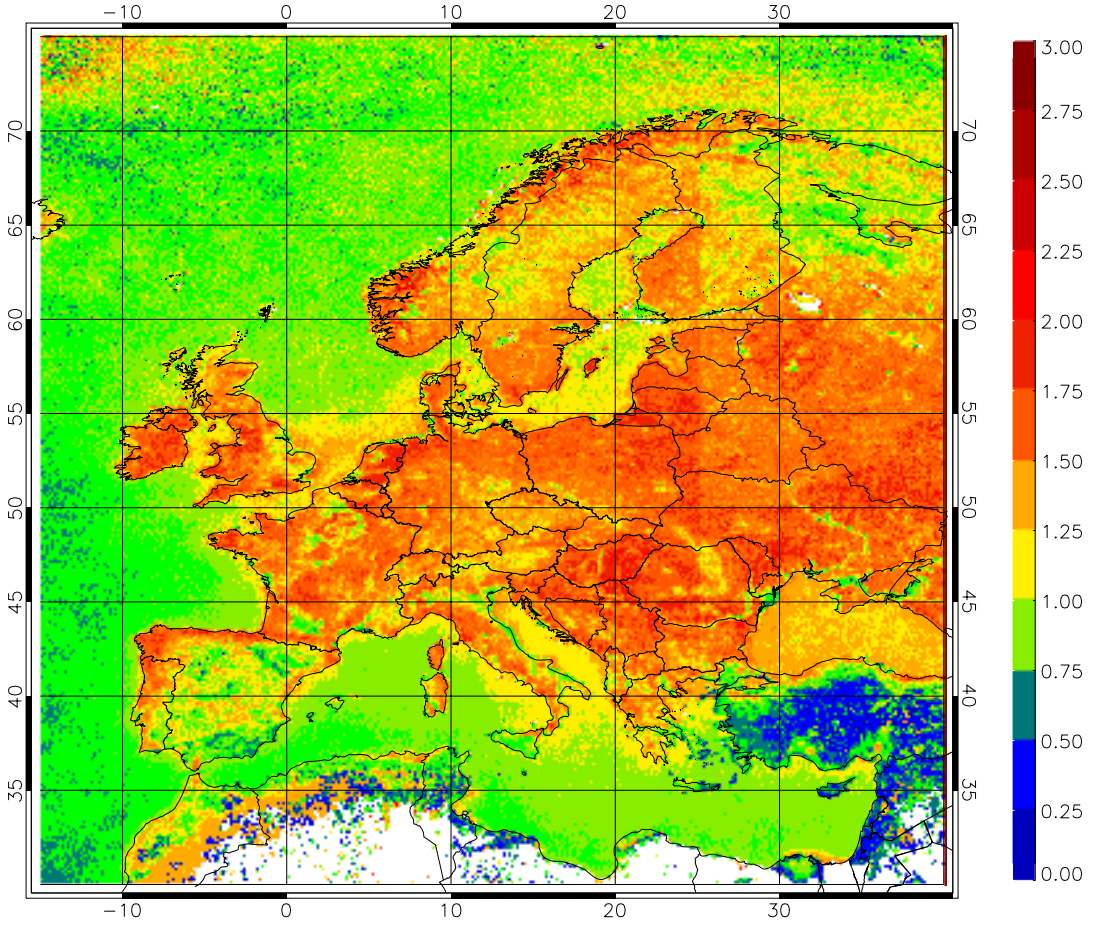

Figure 6.3 Yearly average Ångström-parameter measured by MODIS in 2003.

Yearly average PM_{10} measurements at rural background stations in Europe are shown in Figure 6.4. The PM_{10} data show high values in the Netherlands/Belgium area, in the Po-valley, and the border between Poland and the Czech Republic, similar to the elevated AOT values. The spatial correlation between yearly average AOT (AOT_F) and PM_{10} is 0.58 (0.53), using the 142 rural background stations in AIRBASE with more than 80% data capture in a year. For $PM_{2.5}$, the spatial correlations are higher, and are 0.63 (AOT) and 0.77 (AOT_F), but this is based on 8 points only (i.e., all $PM_{2.5}$ rural background stations available in AIRBASE for 2003).

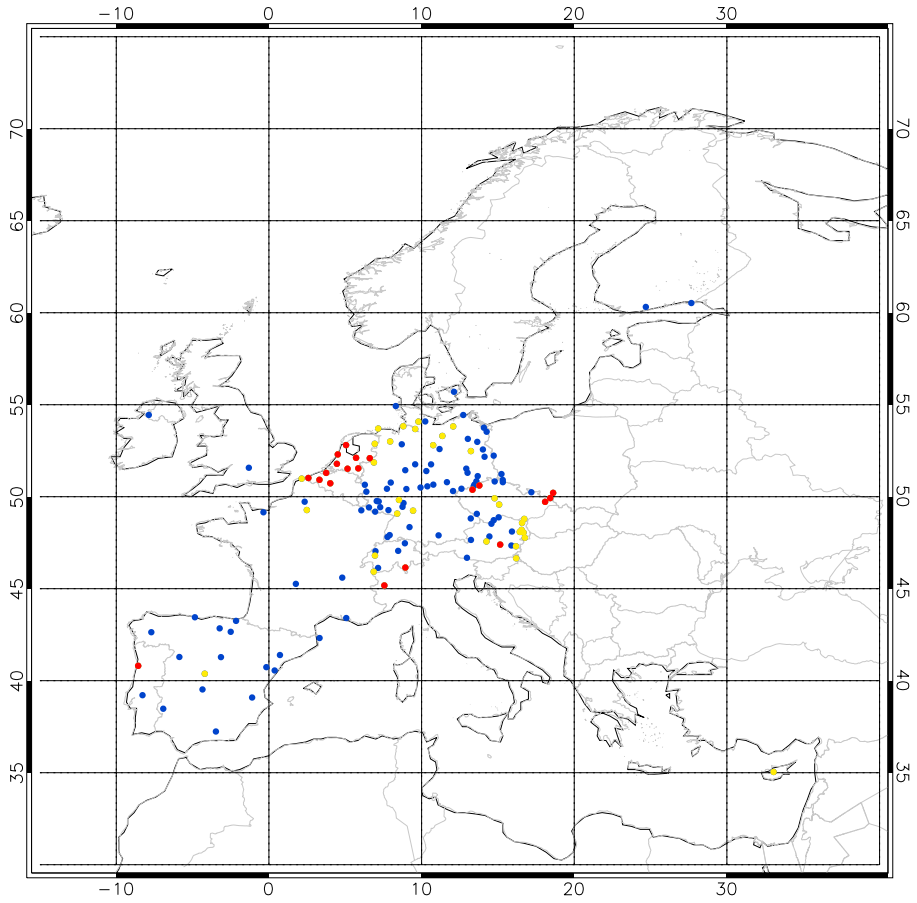

Figure 6.4 Yearly average PM_{10} measurements from AIRBASE, for 2003, at rural background stations. Only stations with more than 80% data capture have been shown. Legend: blue: yearly average PM_{10} < 25 µg/m3; yellow: 25 µg/m3 < yearly average PM_{10} < 32 µg/m3; red yearly average PM_{10} > 32 µg/m3.

The correlations above pertain to yearly average PM data, determined as the average over all days for which PM measurements were available. The satellite measurements of AOT, however, are only available under cloud-free conditions. Under such meteorological conditions, PM values are generally higher than average. Indeed, 90% of the stations show a higher 'yearly average' PM determined by averaging days for which satellite data are available than the true yearly average PM. The average difference (averaged over all stations) between these two methods is about 15% for both PM_{10} and $PM_{2.5}$. Also the spatial correlations were studies using average PM data, calculated as an average over the days for which satellite measurements were available. In general, this did not have much effect on the strengths of the spatial correlations. This is because the general spatial distribution of yearly average PM is rather similar for both methods of calculating a yearly average PM, besides the systematic difference of 15%. For both averaging methods, $PM_{2.5}$ correlates better with AOT_F than with AOT, while PM_{10} shows about equal correlations with AOT and AOT_F.

6.2 Comparison of temporal variations of AOT and PM

Monthly average data for selected regions

Figures 6.5 and 6.6 show the seasonal variation of AOT and PM, respectively, for whole Europe (same area as depicted in Figure 6.1), and for several selected regions: the Netherlands/Belgium, the border region between Poland and the Czech Republic, and Spain/Portugal. The regions were selected because the aerosol sources and composition differ substantially between these regions as well as the average meteorological conditions. Another criterion was the availability of ground-based measurements. The PM measurements shown in Figure 6.6 were performed at rural background stations.

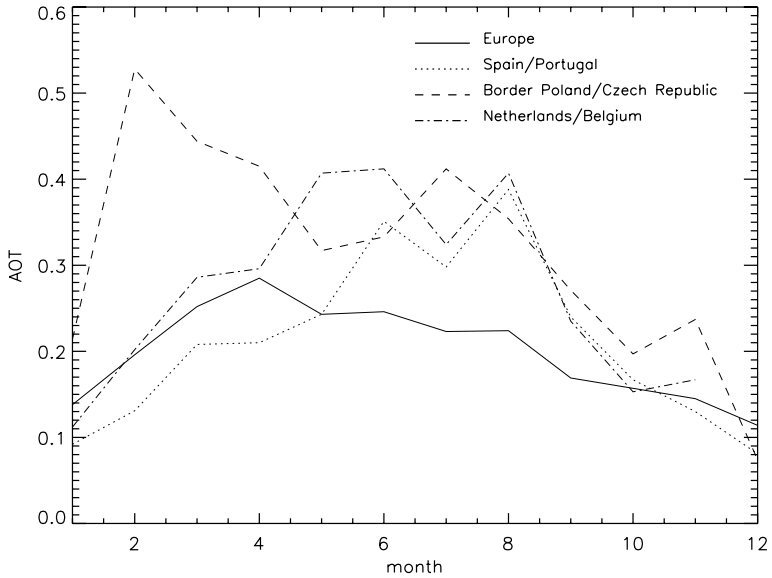

Figure 6.5 Seasonal variation of aerosol optical thickness averaged over Europe and several European regions in 2003.

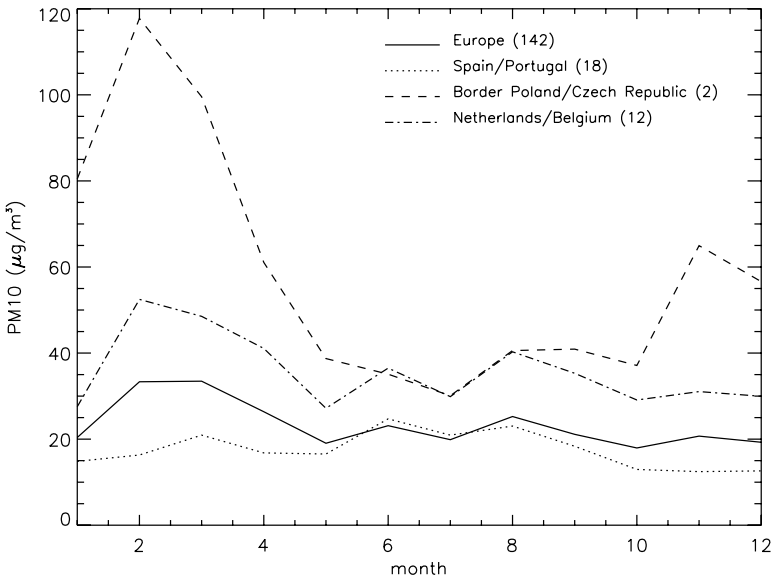

Figure 6.6 Seasonal variation of PM_{10} averaged over all rural background stations in Europe and those in several European regions in 2003. The number of stations in the average is given in brackets.

Table 6.1 Correlations between monthly average AOT, PM, and precipitation for whole Europe and selected areas.

	Whole Europe	Spain/ Portugal	Border Poland/ Czech Republic	Netherlands / Belgium
AOT-PM	0.47	0.88	0.40	0.22
AOT-precipitation	-0.91	-0.83	-0.45	-0.41
PM-precipitation	-0.48	-0.84	-0.45	-0.82

The seasonal variation in PM is generally less pronounced than that of the AOT. We have verified that periods of relatively low AOT and PM correspond to periods with high precipitation and vice versa. Typically both monthly average AOT and PM show anti-correlations with precipitation of between 0.4 – 0.9 for the selected areas (see Table 6.1). In particular, the high peak in both PM and AOT in February for the border region between Central Poland and the Czech Republic corresponds with a very dry period in that area. This suggests that wet removal of aerosols is likely to play an important role in explaining variations of monthly averages of AOT and PM. High precipitation in winter leads to low AOT and PM levels, but in case of PM this may to some extent be offset by lower boundary layer heights in winter, which lead to higher concentrations near the surface. This may explain the generally smaller seasonal variation in PM compared to the AOT.

Daily and hourly average data at individual stations

Daily and hourly time-series have been analyzed in detail for the AIRBASE stations that both measured PM_{10} and $PM_{2.5}$ in 2003. For 86 stations daily average data were available, and for a subset of 28 stations hourly average data were available for (part of) 2003. The corresponding AOT values have been selected from the MODIS images in 2003 above these stations. Correlation coefficients have been calculated between the one-year time-series of AOT and PM. In case of hourly PM data, the measurement closest in time to the satellite measurement was used. For stations with daily average PM data only, the daily average was compared to the (instantaneous) AOT measurement at the same day. Also, meteorological parameters (boundary layer height, relative humidity) were extracted from the ECMWF archive and analysed. Precipitation was not considered in this time-series analysis, as the comparison is limited to cloud-free conditions (as AOT measurements are only possible under cloud free conditions). The 3-hourly ECMWF data were interpolated in time to that of the satellite measurement. Also correlations were calculated with a 'meteo-scaled' optical thicknesses, AOT*, which is defined in this report as

$$AOT^* = \frac{AOT}{BLH\ f(RH)},$$

where BLH is the boundary layer height, and the function f(RH) describes the increase of the aerosol extinction cross-section with relative humidity, and is proportional to the average projected area of the aerosol particles. Although the function f(RH) depends on time and space dependent hygroscopic characteristics of the aerosols (Day et al., 2001), a single uniform function was used in this study, based on measurements by Veefkind et al. (1996). A similar quantity is calculated for AOT_F. In Chapter 2, it was shown that the AOT* is expected to show higher time-correlations with PM than AOT directly. This can be readily understood: by dividing the AOT by the height of the mixing layer, one accounts for the effect of dilution of the surface concentrations due to vertical mixing. By dividing by f(RH) one accounts for the fact that the AOT is measured under ambient (humid) conditions, while PM is determined after heating the air sample, and hence pertains more to the dry aerosol mass. Average

correlation coefficients are presented in Table 6.2 (averaged over different stations). Only time-series with more than 50 points (AOT, PM) have been used to calculate the average.

Table 6.2 Average correlation coefficients of time-series of hourly/daily average PM data with several parameters: AOT, the `meteo-scaled' AOT (AOT), the reciprocal of the boundary layer height (BLH^{-1}) and X^{-1}, where X=BLH f(RH). N indicates the number of stations included in the average. Station characteristics are given in the last column.*

	AOT	AOT*	BLH^{-1}	X^{-1}	N	Station type
Hourly $PM_{2.5}$	0.31	0.60	0.40	0.45	9	Background
	0.22	0.42	0.38	0.37	9	Traffic
	0.38	0.59	0.31	0.39	3	Rural background
Hourly PM_{10}	0.32	0.46	0.24	0.29	10	Background
	0.17	0.34	0.25	0.25	11	Traffic
	0.39	0.54	0.21	0.30	3	Rural background
Daily $PM_{2.5}$	0.18	0.46	0.38	0.43	53	Background
	0.21	0.44	0.38	0.41	22	Traffic
	0.27	0.48	0.33	0.39	8	Rural background
Daily PM_{10}	0.21	0.41	0.27	0.34	54	Background
	0.15	0.39	0.31	0.37	26	Traffic
	0.35	0.44	0.18	0.25	8	Rural background

From Table 6.2 it can be observed that the direct time-correlation of PM and AOT for a whole year is low (0.3). This largely reflects the different seasonal behaviour of PM and AOT. Besides precipitation, which affects both PM and AOT, the temporal variation of PM is strongly influenced by that in BLH. BLH^{-1} even shows a higher correlation with PM than the AOT. It is interesting to note that the parameter $(BLH\ f(RH))^{-1}$ shows even higher time-correlations, while no significant correlation is found between PM and 1/f(RH) (not shown). Apparently, relatively low PM values are measured under circumstances of both high relative humidity and high BLH, and vice versa. A straightforward explanation for a higher correlation of PM with $(BLH\ f(RH))^{-1}$ than with BLH^{-1} was not found.

As might be expected, the highest time-correlation is found using the meteo-scaled optical thicknesses, AOT*. Also the time-correlations were studied between PM and AOT_F*. These correlations were found to be essentially identical as those with AOT (not shown).
Not surprisingly, the time-correlations are higher using hourly averaged PM data rather than daily average PM data. A correlation of 0.6 is found between AOT* and $PM_{2.5}$, using hourly data of $PM_{2.5}$ (closest to time of satellite overpass) at rural background stations. For PM_{10}, the correlation (0.5) is lower than for $PM_{2.5}$. Background stations (urban, suburban, and rural) show higher correlations than traffic stations, as background stations are more representative of the 10x10 km^2 area observed by the satellite.

The results shown in Table 6.2 are based on all AOTs retrieved from MODIS, irrespective of the cloud fraction in the 10x10 km^2 pixel. This cloud fraction is reported in the MODIS data product as well. The dependence of the correlation between PM and AOT on this reported cloud fraction has been investigated as well. It turns out that, as might be expected, the correlation improves when only (AOT, PM) pairs are considered that pertain to completely

cloud-free conditions. In that case, the correlation between AOT* and hourly data of $PM_{2.5}$ is 0.77, and for AOT* and hourly data of PM_{10} is 0.68.

6.3 Statistical mapping of particulate matter

In this section, results are presented of the statistical approach to map $PM_{2.5}$ and PM_{10}. In this statistical approach, measured PM concentrations are interpolated over Europe using spatial variations that are derived from 'explanatory fields'. Here, two explanatory fields are used: (1) the AOT (or AOT_F) fields derived from MODIS, and (2) $PM_{2.5}$ concentrations that were modeled using the LOTOS-EUROS model (PM_{LE}). In section 6.2, it was shown that scaling of the AOT with boundary layer height and relative humidity substantially improves the time-correlation with PM, as day-to-day variations in boundary layer height and relative humidity influence PM and AOT levels. It was found that such a scaling worsens the spatial correlation of the yearly averages, however. The reason is that yearly average boundary layer height or atmospheric humidity is not clearly related to PM concentration levels. For example, the boundary layer is, on average, higher in Southern Europe than in Northern Europe, while AOT and PM levels do not show corresponding lower PM or AOT levels in Southern Europe. Therefore, mapping yearly average PM based on a meteo-scaled AOT or AOT_F is not performed.

The following form has been adopted to map PM:

$$PM_{fit} = a_1 AOT_{MOD} + a_2 PM_{LE} + a_3,$$

where PM_{fit} is the PM concentration obtained through statistical fitting of the AOT or AOT_F derived from MODIS (denoted by AOT_{MOD}), and the $PM_{2.5}$ concentrations modelled with the LOTOS-EUROS model (denoted by PM_{LE}). The coefficients a_1, a_2, a_3 are free-parameters in this model, and have been fitted through least-squares minimization of PM_{fit} (evaluated at measurement locations) and measured concentrations of $PM_{2.5}$ (or PM_{10}) concentrations. For this minimization, the Levenberg-Marquart algorithm is used. The $PM_{2.5}$ concentrations modelled by LOTOS-EUROS are also used as an explanatory field for PM_{10} concentrations, rather than PM_{10} concentrations modelled by LOTOS-EUROS. However, modelled PM_{10} does not differ much from modelled $PM_{2.5}$, as many natural sources that contribute to PM_{10} are not accounted for in the emission inventories used by LOTOS-EUROS.

The fitting is performed using rural background stations that have more than 80% data capture during 2003. This amounts to 142 PM_{10} stations, and, unfortunately, only 8 $PM_{2.5}$ stations in AirBase. The $PM_{2.5}$ stations in AirBase are predominantly located in Central Europe. To obtain a more equal distribution of stations in the fitting region (whole Europe), also five EMEP $PM_{2.5}$ rural background stations were added for the final analysis (three in Scandinavia and two in Spain). The results presented here apply to fitting to this final set of 13 $PM_{2.5}$ stations, as listed in Table 6.5.

Initially, for PM_{10}, the dataset was arbitrarily divided into a 'calibration set' (used for the fitting, 50% of the stations), and a 'validation set' (used for validation of the fitted relation, other 50% of the stations). It turned out that the results (error statistics) were very similar for the validation and calibration sets, and therefore, the final fitting analysis was done using the whole dataset. For $PM_{2.5}$, the small amount of data points prohibited a division into a calibration and validation set, and the fitting was done for the whole dataset only. However, it

is likely that $PM_{2.5}$ statistics would have behaved similar to PM_{10} in this respect, i.e., little difference in performance between validation and calibration subsets.

Table 6.3 Error-statistics for fitting the explanatory fields to observed spatial variations in yearly average concentrations of $PM_{2.5}$ and PM_{10} at rural background stations in Europe. Units: $\mu g/m^3$ (mean error, root-mean-square (RMS) error, mean absolute error.

	$PM_{2.5}$	**PM_{10}**	**Explanatory fields**
Mean error	-0.53	-0.78	LOTOS/EUROS only
RMS error	3.67	8.08	
Mean abs. error	3.10	5.57	
Correlation coeff.	0.70	0.58	
Mean error	0.14 (0.12)	-0.21 (-0.01)	MODIS only; results using AOT_F (AOT)
RMS error	3.40 (3.81)	8.13 (7.75)	
Mean abs. error	2.29 (2.75)	5.81 (5.68)	
Correlation coeff.	0.72 (0.61)	0.53 (0.58)	
Mean error	0.17 (0.00)	-0.07 (0.13)	LOTOS-EUROS and MODIS; results using AOT_F (AOT)
RMS error	2.82 (3.09)	7.44 (7.10)	
Mean abs. error	2.11 (2.42)	4.94 (4.85)	
Correlation coeff.	0.82 (0.76)	0.63 (0.67)	

Table 6.3 shows the error-statistics when MODIS measurements of yearly average AOT and AOT_F and/or yearly average LOTOS-EUROS fields of $PM_{2.5}$ are fitted to observed yearly average concentrations of $PM_{2.5}$ and PM_{10} at rural background stations in Europe. This table describes, in a statistical sense, the difference between observed PM levels and PM_{fit}. The mean errors are - by definition - close to zero, as this is minimized during the fitting procedure. It is apparent that for PM_{10}, fitting with the AOT gives slightly higher spatial correlations than with AOT_F, while for $PM_{2.5}$, the opposite is true: fitting-errors are smaller using AOT_F than AOT. This is a plausible result, because $PM_{2.5}$ and AOT_F are both dominated by the smaller particles. By using both explanatory fields the correlation between fitted and measured PM fields improves compared to fitting with just one explanatory field. Using the two explanatory fields, the RMS-errors reduce by 25% for both $PM_{2.5}$ and 10% for PM_{10}. The final spatial correlation coefficients are 0.82 for $PM_{2.5}$ and 0.67 for PM_{10}. The statistics for $PM_{2.5}$ is not very robust, however, because it is based on 13 stations only. The fitting results for the coefficients a_1 (unit: $\mu g/m^3$), a_2 (dimensionless) and a_3 (unit: $\mu g/m^3$) are listed in table 6.4. In the top rows, the fit was forced through (0,0), while in the bottom rows also the coefficient a_3 is fitted. It can be observed that for $PM_{2.5}$, the map obtained using fitting with both LOTOS-EUROS and MODIS is for 45% based on LOTOS-EUROS and for 55% on MODIS, and also for PM_{10}, the weights are about equal for both explanatory fields.

Table 6.4 Fit-coefficients pertaining to fitting $PM_{2.5}$ with LOTOS-EUROS and MODIS field only, and combined. Top rows: fit forced through (0,0), bottom: a_3 is also fitted.

	$PM_{2.5}$			PM_{10}		
	a_1	a_2	a_3	a_1	a_2	a_3
Lotos-Euros only	0	1.39	0	0	2.16	0
Modis only, AOT_F (AOT) for $PM_{2.5}$ (PM_{10})	57.6	0	0	94.2	0	0
Lotos-Euros and Modis	33.1	0.63	0	53.6	0.97	0
Lotos-Euros only	0	0.98	3.87	0	1.53	7.45
Modis only, AOT_F (AOT) for $PM_{2.5}$ (PM_{10})	70.9	0	-2.89	89.1	0	3.56
Lotos-Euros and Modis	48.7	0.65	-3.61	48.0	1.09	1.27

Table 6.5 Yearly average values of measured and modelled $PM_{2.5}$, AOT_F, and fitting results for $PM_{2.5}$ using LOTOS/EUROS (LE), MODIS, and both LOTOS/EUROS and MODIS, at rural background stations in 2003. The last column lists the difference between measured and fitted $PM_{2.5}$ using both LE and MODIS.

Station	Technique	lat	lon	Meas. $PM_{2.5}$	Model $PM_{2.5}$	Meas. AOT_F	Fitted $PM_{2.5}$		
							LE only	Modis only	LE & Modis
AT0002R	gravimetry	47.8	16.8	24.7	12.2	0.30	16.9	19.1	18.9
DE0002R	gravimetry	52.8	10.8	16.5	10.1	0.32	13.9	20.1	19.1
DE0003R	gravimetry	47.9	7.9	10.2	9.9	0.20	13.8	12.5	12.8
DE0004R		49.8	7.1	13.8	10.6	0.17	14.7	10.7	11.6
DE0737A	β-absorption	49.3	7.8	12.5	9.2	0.19	12.7	11.9	12.5
GB0036R	TEOM	51.6	-1.3	11.8	10.8	0.19	14.9	12.3	13.0
GB0617A	TEOM	51.5	0.6	12.5	12.3	0.23	17.1	14.5	15.2
PT0128A	β-absorption	39.2	-8.3	9 .9	4.4	0.17	6.1	10.8	10.0
NO0001R		58.4	8.3	5.0	2.4	0.21	3.4	11.9	8.4
NO0099R		58.1	6.7	7.3	2.8	0.15	3.9	8.9	6.9
SE0011R		56.2	13.2	10.5	8.8	0.22	12.2	12.9	12.9
ES0008R		43.4	-4.9	11.0	5.0	0.20	6.9	11.4	9.6
ES0016R		43.2	-7.7	9.3	8.4	0.19	11.6	10.8	11.5

Our primary interest in this study is mapping $PM_{2.5}$. Also the results of the statistical mapping are more promising for $PM_{2.5}$ than for PM_{10}. For these two reasons, the discussion is limited to $PM_{2.5}$ in the remainder of this section. Table 6.5 lists the measured $PM_{2.5}$ and fitted $PM_{2.5}$, as well as the values of the explanatory variables at these location. The applied calibration factors applied to the measurements are unknown for $PM_{2.5}$. Figure 6.7 a-c show the fitted fields for $PM_{2.5}$, using only LOTOS-EUROS as explanatory variable, using only the AOT_F filed as explanatory variable, using both explanatory fields. For these map, the fits were forced through (0,0). It can be observed that, comparing the two top maps, the large scale patterns resemble each other. It is apparent that the model-based map shows larger spatial contrasts between clean and polluted regions, and also cities are more clearly distinguishable in the modelled map. Nevertheless, major individual cities are also distinguishable in the MODIS-based map, as was noted and discussed in Section 6.2. Also it can be observed that the MODIS-based field shows higher values in Eastern Germany and Poland compared to the model-based field. When analysing monthly and seasonal images (see appendix A), it turns out that this feature is particularly apparent in the winter and spring, but it is also present in July. This might point to higher aerosol emissions in reality than assumed in the emission inventory that used for the model calculations (perhaps related to the use of stoves for domestic heating), but also other explanations, not related to emissions, are possible, such as contamination of the AOT_F field by patches of snow. Also, it is apparent that the model-based map gives lower $PM_{2.5}$ concentrations in Scandinavia compared to Spain, while the MODIS-based map is higher in Scandinavia compared to Spain, i.e., opposite behaviour. The measured high values of AOT_F in high up in Scandinavia are probably unrealistic, as aerosol sources are far away. It is more likely to be a measurement artefact, e.g., contamination by patches of snow. This is suggested by the seasonal variation of the AOT in Scandinavia, with particularly high AOT_F values only occurring in spring (see Appendix A). The relatively high AOT_F-values in Portugal (as compared to Spain) only occurred in the summer, and are likely to be due to the large forest fires in Portugal in summer 2003. These rather unpredictable emissions from biomass burning are not included in the emission inventories and do not show up in the modelled field. As noted above, the fitted map using both explanatory fields (bottom) resembles about equally the features of the modelled $PM_{2.5}$ map and the AOT_F map.

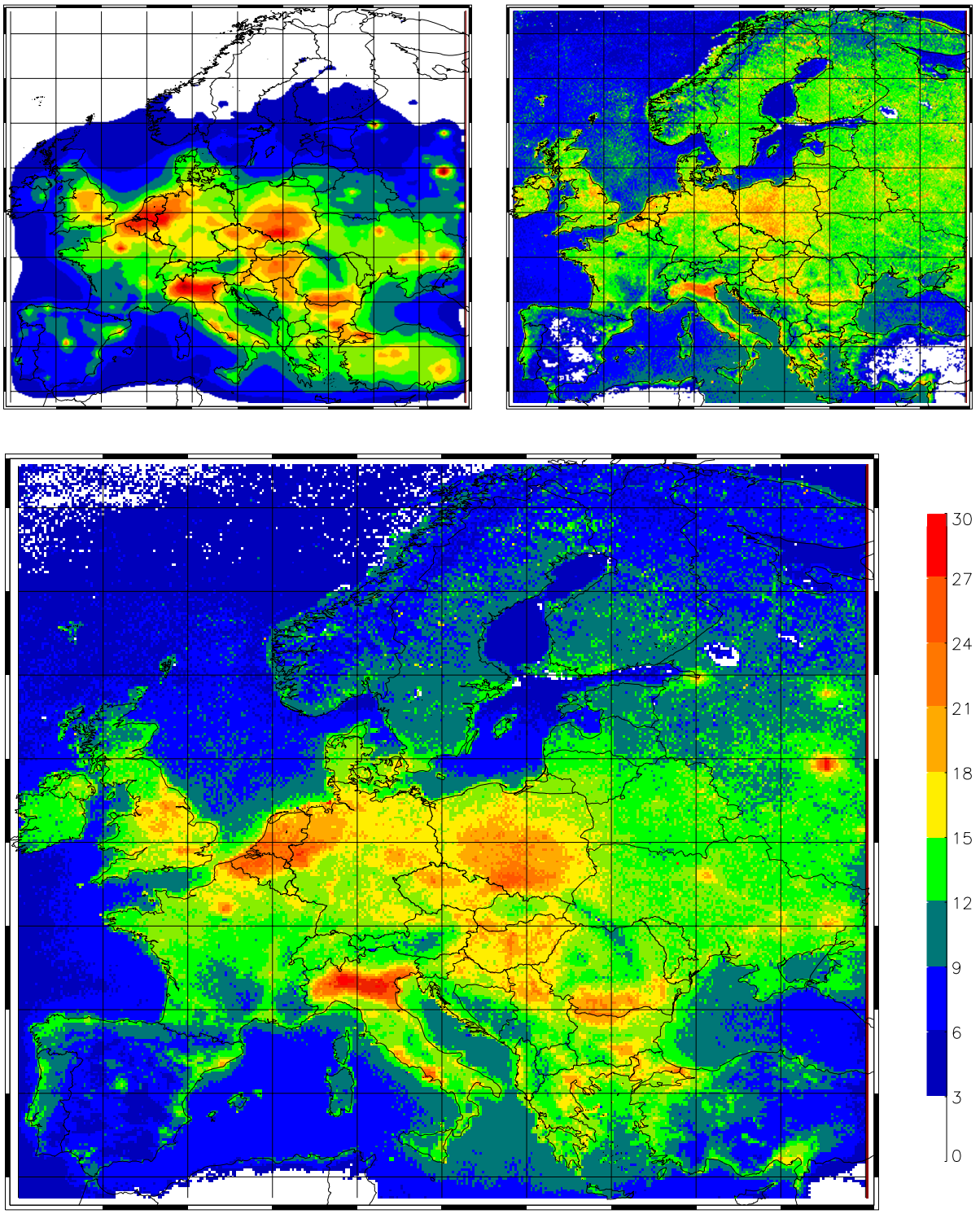

Figure 6.7 Fitted fields for $PM_{2.5}$ using only LOTOS/EUROS as explanatory variable (top left), using only the AOT_F filed as explanatory variable (top right), using both explanatory fields (bottom, large). For these map, the fits were forced through (0,0). All maps have the same colour scale.

7. Mapping of $PM_{2.5}$ – assimilation approach

7.1 Set-up of the assimilation experiment

Observations of aerosol optical thickness (or any other component) consist of data that are irregularly distributed in space and time. Data assimilation allows the calculation of continuous fields in space and time from observations that are irregularly distributed. Data assimilation consists of making a best estimate of the state of the atmosphere on the basis of observations and a model prediction of the atmospheric state both of which have associated errors. Data assimilation basically defines a new atmospheric state by making a weighted average of the observed and modelled state in an intelligent and statistically sound way. Hence, if a model value is more uncertain than an observed value, more weight will be put on the observation, and the assimilated value will tend to get closer to the observed value and vice versa (see Figure 7.1).

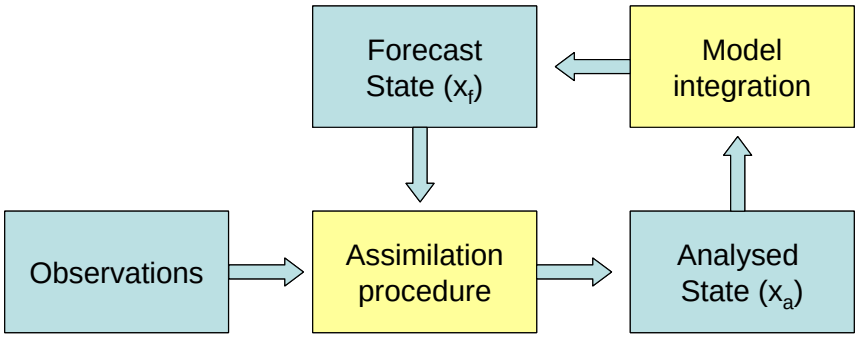

Figure 7.1 Schematic representation of the data assimilation procedure.

In this study an ensemble Kalman filter approach was used to assimilate the AOT retrievals within LOTOS-EUROS. The uncertainties involved with the modelled and retrieved AOT values determine the weights that are put on the measured and calculated values. With a Kalman filter there is no need to specify the model uncertainties as they are determined by the range of modelled states of the ensemble members. Hence, the specification of the noise influences the weights and therewith results of the procedure. Here, an ensemble size of 15 ensemble members was used. Random noise was added to the emissions of NO_x, SO_x, VOC, NH_3 and particles and to the dry deposition sink. All noise factors were applied with a mean of 1 and a standard deviation of 0.25. Hence, the vast majority for the factors are within the range of 0.5 to 1.5. All noise factors were set after an assimilation step and held constant until the next assimilation step. The MODIS TERRA and AQUA overpasses take place around 10:30 and 13:30 local time every day. In the model the analysis is performed at 12:00 hours GMT and all ensemble members have disturbed but constant emissions for the 24 hours in between overpasses. At noon, the AOT is calculated for the grid cells for which observations are available and the state and ensemble members are updated in the analysis step.

As stated above the uncertainties associated with the measurements are important to know. Based on the validation of MODIS data against AERONET, it was decided to use MODIS AOT_F*0.9 over MODIS AOT in this assimilation study. The reason is that this quantity closely resembles the characteristics of a normally distributed error. Hence, all MODIS AOT_F data were multiplied by a factor 0.9 to correct for the average bias in these data compared to AERONET. Both the MODIS data from the AQUA as from the TERRA satellite have been

used. Before assimilating the measurements in the model, the measurements are redistributed onto the LOTOS-EUROS grid of 0.5°x0.25°.
The assimilation was carried out for a full year, i.e. 2003. The simulation was carried out on a domain that incorporates central Europe. The domain is slightly reduced compared to the normal LOTOS-EUROS model domain for two reasons. Firstly, the assimilation for a full year (with 15 ensemble members) requires a very large computational effort. Hence, eliminating less interesting areas, such as the (clean) northern part of Scandinavia, reduces the computational effort. Secondly, our model does not incorporate (desert) dust which significantly contributes to AOT in southern Europe.

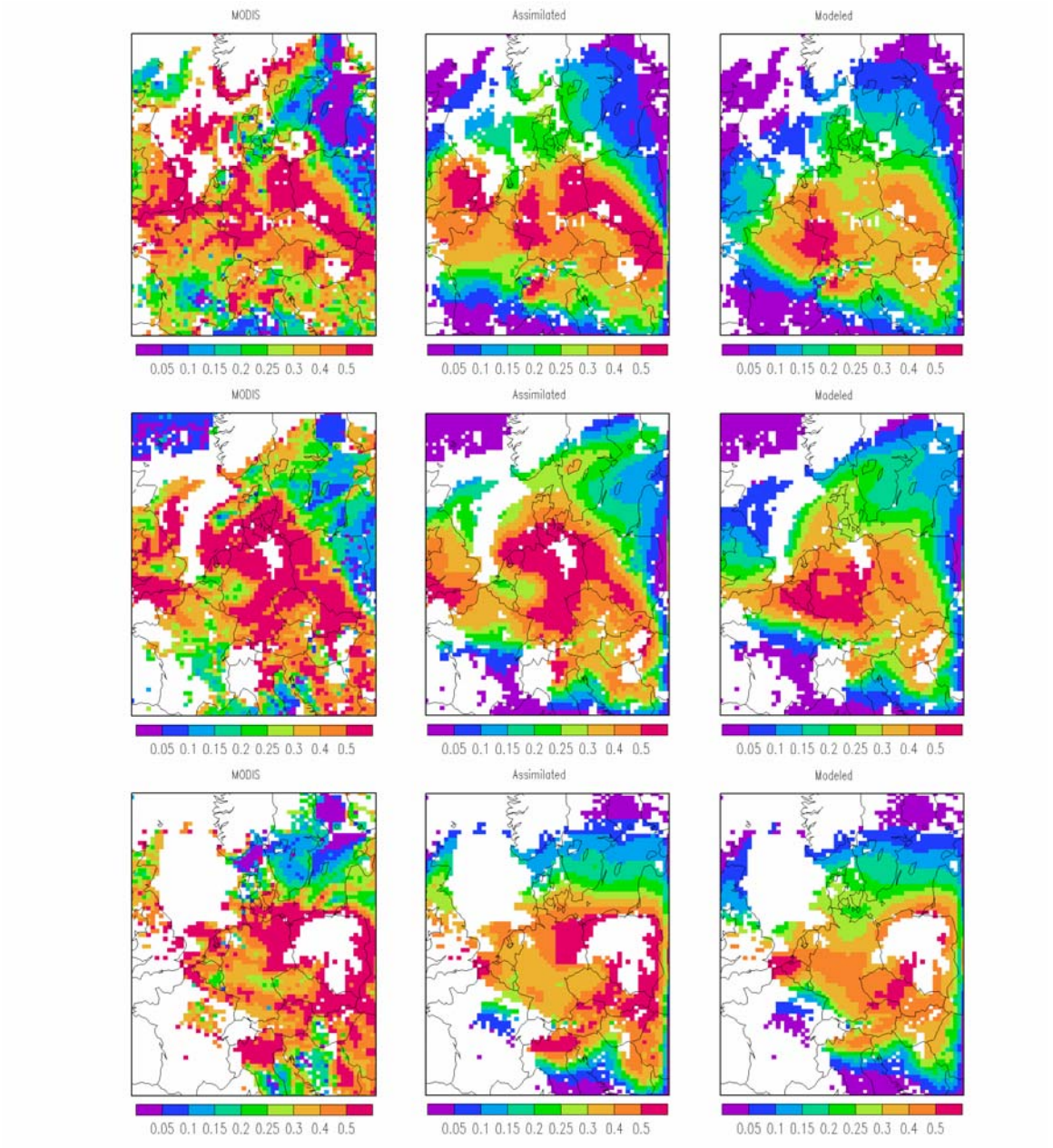

*Figure 7.2 MODIS AOT_F (left), assimilated AOT_F*0.9 (middle) and modelled AOT (right) fields for 26 (top row), 27 (middle row) and 28 (bottom row) March 2003.*

7.2 AOT assimilation results and validation with AERONET

For this study, one year of MODIS AOT data for 2003 have been assimilated into the LOTOS-EUROS system. Daily fields of retrieved, modelled and assimilated AOT have been inspected visually. The picture arises that there are two situations that can be distinguished. The first situations show promising results. On the other hand, the second group of days shows low improvements due to the assimilation.

Figure 7.2 shows the measured (not bias corrected), modelled and assimilated fields for three consecutive days (26-28 March 2003). For all days the modelled field compares rather well with the retrieved AOT distribution. Overall, the modelled AOT values are somewhat lower than the MODIS data. Through the assimilation, the structures in the retrieved field are strengthened in the model state. Furthermore, the residue is reduced. Hence, these days characterized by low cloud cover are examples of cases where the assimilation gives promising results.

Figure 7.3 shows the results of the assimilation on a cloudy day. The model predicts low AOT whereas considerably high AOT values are retrieved. The assimilation closes the gap for about 50%. The map of the retrieved nicely illustrates the problem of cloud contamination. A large number of cells show high AOT where all neighbouring cells have been recognized as cloud contaminated. On the other hand, the AOT in these cells are equal or lower than those over Hungary. Furthermore, also the shorelines along the Adriatic sea are visible in the AOT, which may be due to spectral mixing of water and land surfaces in the retrieval, and reflections of suspended matter in the shallow water (Koelemeijer et al., 2006). They do not show up in the assimilated picture.

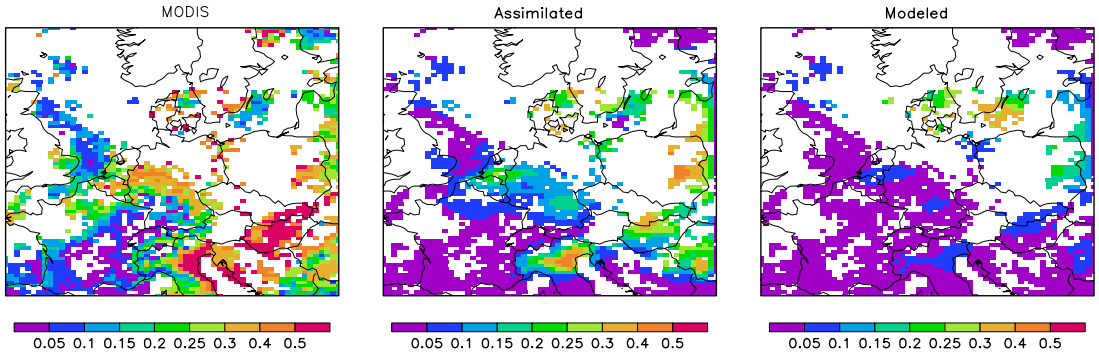

Figure 7.3. MODIS AOT_F (left), assimilation (middle) and modelled AOT (right) fields for a cloudy day (May, 2).

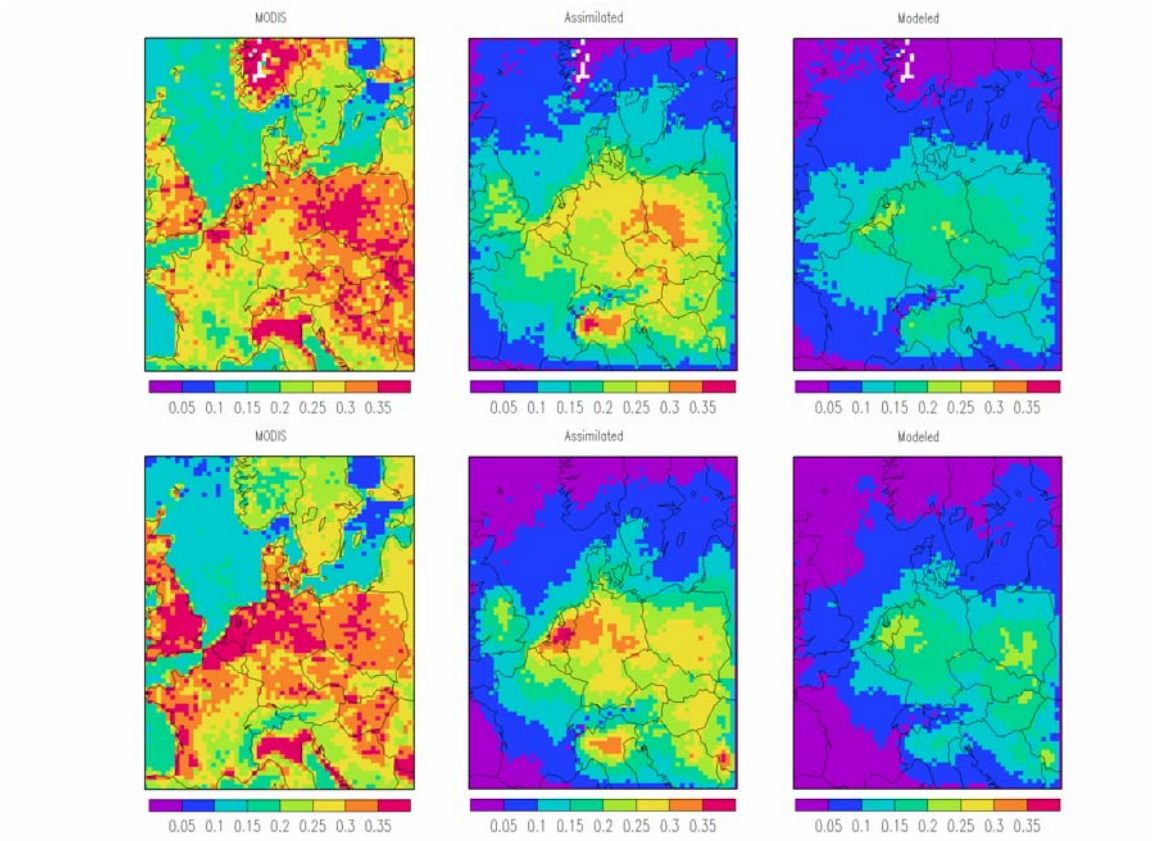

*Figure 7.4 Seasonal averaged fields of MODIS AOT_F (left panels), LOTOS EUROS AOT (right panels) and from the assimilation of MODIS AOT_F*0.9 in LOTOS-EUROS (middle panels). Top row: March-April-May. Bottom row: June-July-August.*

Figure 7.4 presents the seasonal averaged results of the assimilation of MODIS AOT_F*0.9 in the LOTOS-EUROS model. The systematic underestimation of the retrieved AOT by the model can clearly be seen and is discussed below. Using assimilation, the gap between modelled and measured AOT is decreased considerably. At the boundaries of the model domain the assimilation is not effective due to the low emissions in those regions and the fixed boundary conditions in the model. Noise factors were not added to the boundary conditions, which leads to a small spread in the ensemble and thus a small uncertainty in the model close to the boundaries.

For validation, the assimilated AOT fields are compared to measurements from the independent ground based AERONET network. In Figure 7.5 the modelled, assimilated and AERONET time series of AOT are shown for the stations The Hague in the Netherlands and Oostende in Belgium. The modelled AOT captures most of the observed peak values, although it often underestimates the observed peak value. The agreement between the modelled AOT and AERONET AOT has improved after assimilation of MODIS measurements, both in absolute value as in timing.

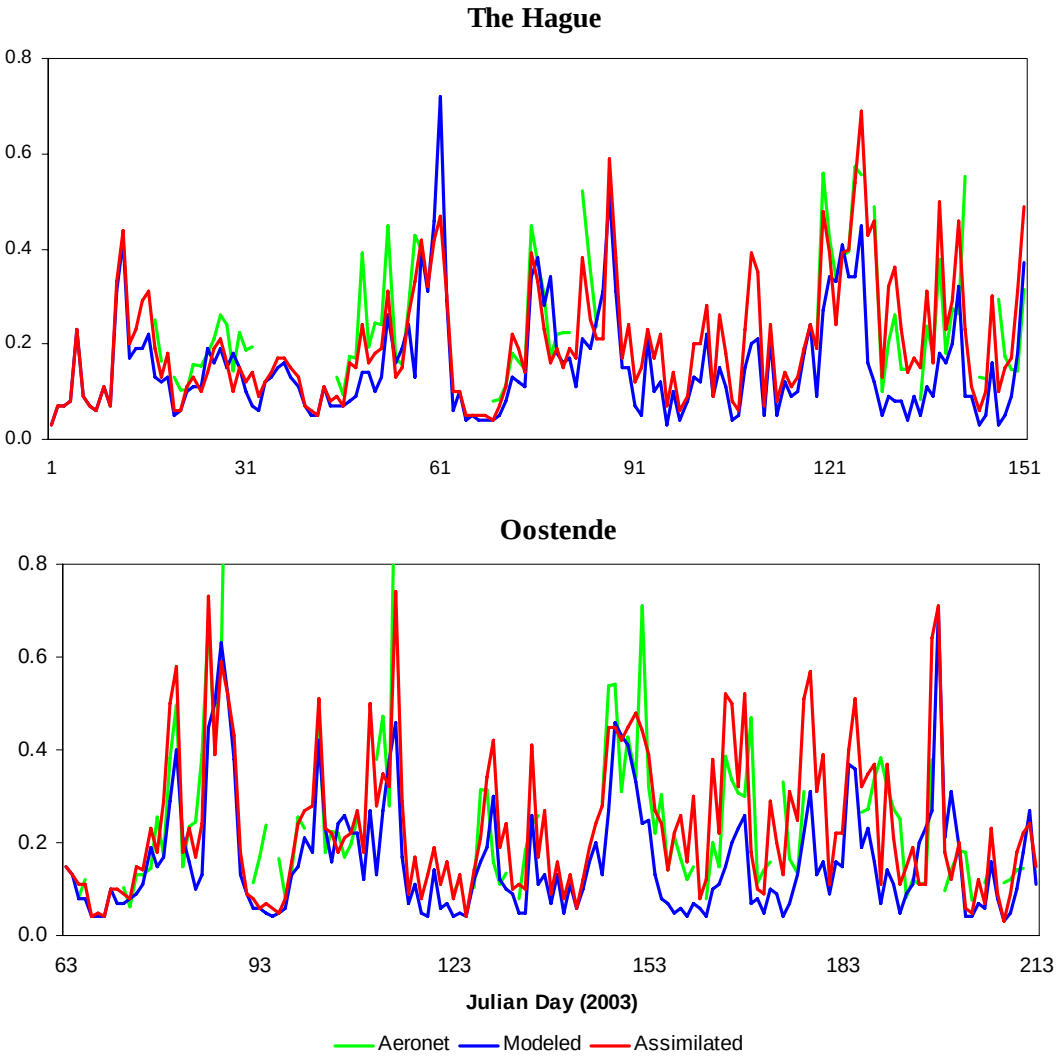

Figure 7.5 Modelled AOT (blue), assimilated AOT (red) and independent AERONET AOT (green) for the station The Hague in the Netherlands (upper panel) and Oostende in Belgium (lower panel) as function of the day number in 2003.

In some cases the good absolute agreement between assimilated AOT values and AERONET is a coincidence, as is illustrated for ISDGM-CNR in Figure 7.6. For this site in Italy, MODIS largely overestimates the AERONET AOT values, while the model largely underestimates the AERONET values. The assimilation of MODIS AOT_F in the model leads to AOT values in between the model and MODIS values, which are by coincidence close to the AERONET data. Although the absolute agreement is coincidence, the improvement in the timing expressed as correlation coefficient is rather insensitive to the absolute (bias in) AOT.

From the validation with AERONET AOT data it is concluded that an important benefit of the assimilation is the improvement of the timing. Except for one station, the time-correlation between modelled AOT and AERONET increases when assimilating the MODIS data (see figure 7.7). The improvement in correlation in some cases is very large.

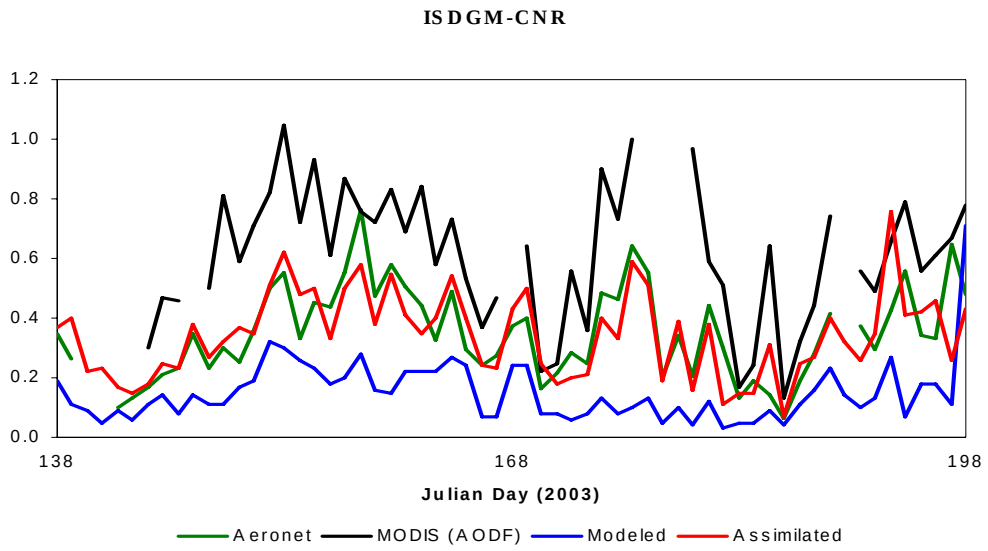

Figure 7.6 Modelled AOT (blue), assimilated AOT (red), MODIS AOT_F (black) and AERONET AOT (green) for the station ISDGM-CNR in Italy, as function of the day number in 2003.

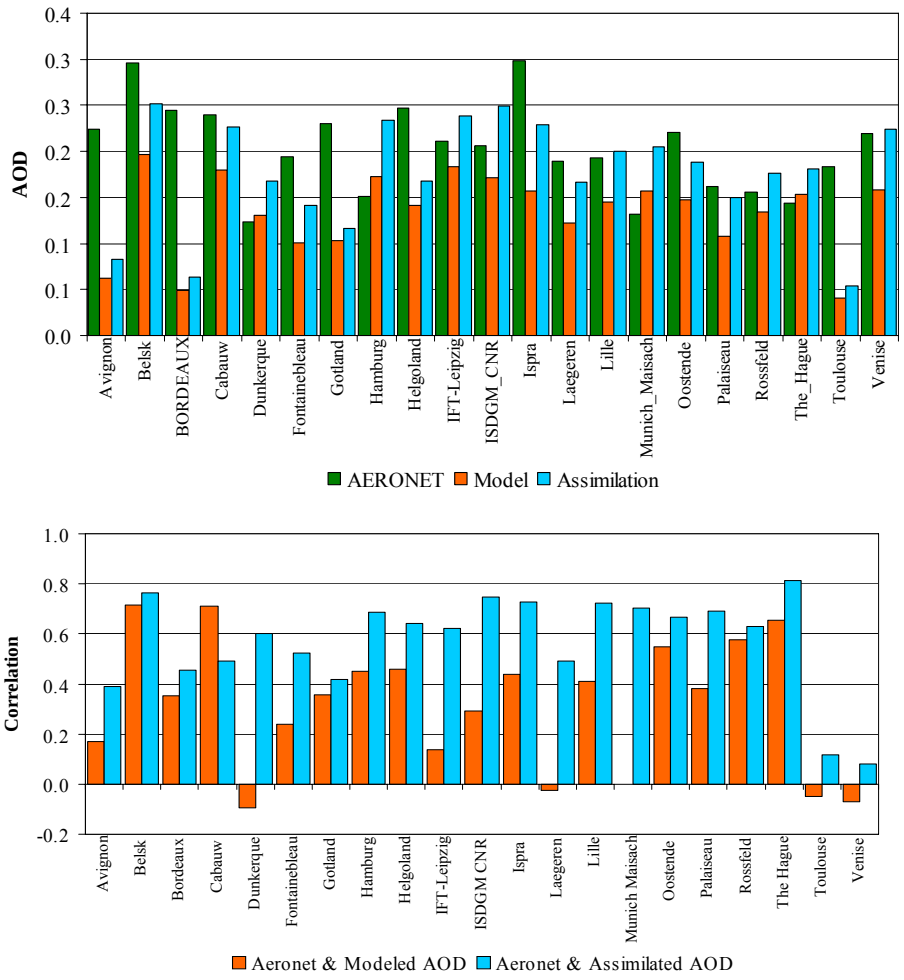

Figure 7.7 Upper panel: Comparison of annual average AOT at 21 AERONET sites. Lower panel: Correlation coefficients between AERONET and modelled AOT and assimilated and AERONET AOT for 21 AERONET stations.

7.3 Derived $PM_{2.5}$ fields

The assimilation of AOT leads to an adapted model state and consequently to changed concentration fields of modelled aerosol components. The fine mode aerosol components are summed to arrive at $PM_{2.5}$. Figure 7.8 shows the effect of the assimilation of MODIS AOT_F*0.9 on the mean $PM_{2.5}$ field for 2003 and the summer of 2003. Through the assimilation the mean $PM_{2.5}$ levels are increased by about 2-3 µg (up to 50%) in central Europe. Also, the gradients are adjusted. For instance, in the Po-valley the model shows enhanced PM levels around Milan, whereas after assimilation the $PM_{2.5}$ distribution in the Po-valley is more even. Furthermore, $PM_{2.5}$ levels in northern Germany have increased more than in the south (west) of the country.

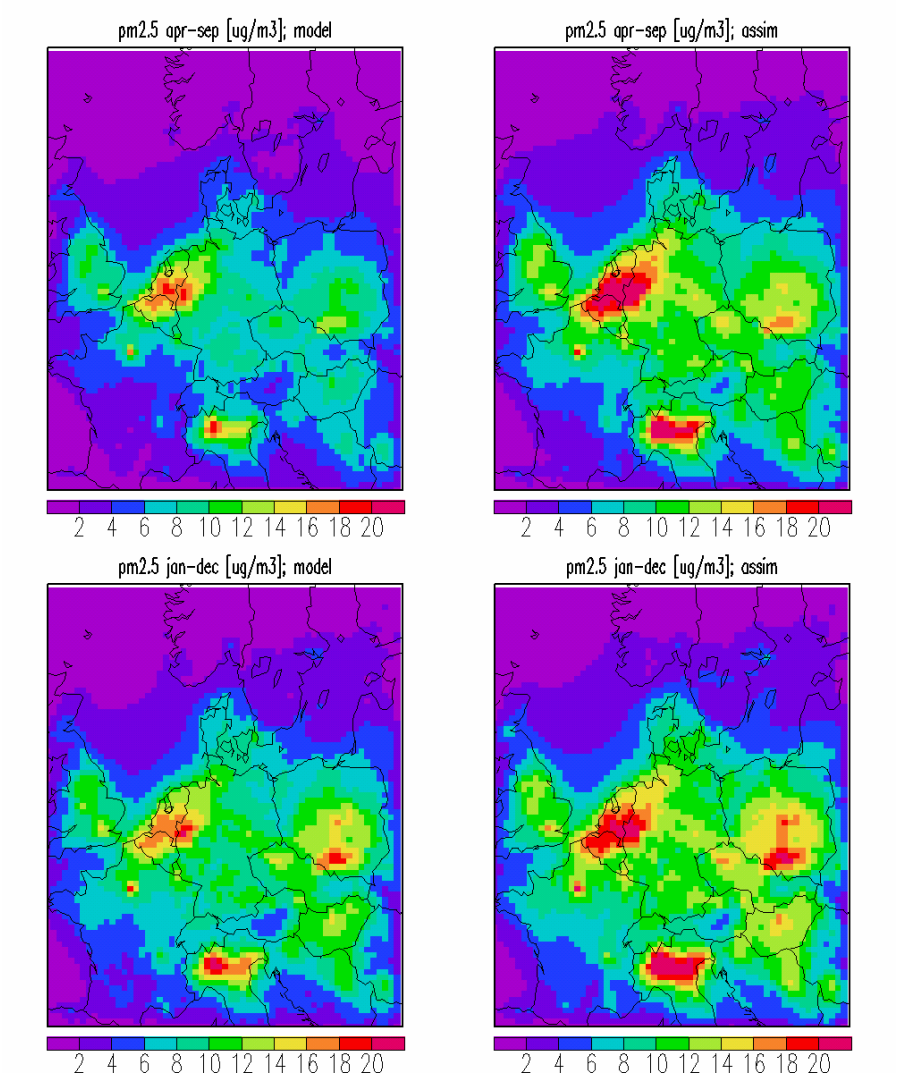

Figure 7.8 PM2.5 fields (in µg/m3) from LOTOS-EUROS before (left) and after assimilation (right) of MODIS AOT fine values averaged over the summer 2003 (top) and the whole year 2003 (bottom).

Validation of modelled $PM_{2.5}$ fields is hampered by the lack of stations in Europe measuring $PM_{2.5}$ concentrations. When properly validating modelled fields with a resolution of 0.5°x0.25°, corresponding to approximately 25x25km^2, only regional background stations should be taken into account. For 2003, only 7 of such regional background stations provided

$PM_{2.5}$ data in AIRBASE for the region concerned. To increase the number of stations in the comparison, also the five EMEP stations in the region considered were used in the analysis. Table 7.1 summarises the modelled and assimilated $PM_{2.5}$ concentrations for these regional background stations.

Table 7.1 Yearly average values of $PM_{2.5}$ for the model and assimilation experiment in comparison to observations at rural background stations in 2003.

Station	lat	lon	Meas. $PM_{2.5}$	LE – model	LE – assim	Residue model	Residue assim
AT0002R	47.8	16.8	24.7	10.9	12.7	13.8	12
DE0002R	52.8	10.8	16.5	9.1	11.3	7.4	5.2
DE0003R	47.9	7.9	10.2	8.6	7.8	1.6	2.4
DE0004R	49.8	7.1	13.8	9.4	11.14	4.4	2.66
DE0737A	49.3	7.8	12.5	8.0	9.4	4.5	3.1
GB0036R	51.6	-1.3	11.8	8.9	10.1	2.9	1.7
GB0617A	51.5	0.6	12.5	10.9	12.24	1.6	0.26
IT0004R	45.8	8.6	28.5	15.4	18.4	13.1	10.1
NO0001R	58.4	8.3	5.0	2.2	2.6	2.8	2.4
NO0099R	58.1	6.6	7.3	3.0	3.5	4.3	3.8
SE0011R	56.0	13.2	10.5	6.0	7.1	4.5	3.4
SE0012R	58.8	17.4	4.8	3.5	4.0	1.3	0.8

The comparison shows that the modelled concentrations are about 30% lower than the measured values. All stations, except DE003R, show a higher mean assimilated $PM_{2.5}$ concentration than the modelled concentration. For these stations the gap between observed and simulated $PM_{2.5}$ is reduced by 10-40%. The spatial correlation for $PM_{2.5}$ is 0.88 for the modelled field, and increases to 0.91 for the field based on the assimilation of AOT. Hence, the assimilation of AOT does provide a better agreement with the ground based measurements of $PM_{2.5}$, although still large absolute differences exist.

Proper validation of the modelled $PM_{2.5}$ fields is not only restricted by the low number of available ground based measurements but also by the quality of the ground based measurements of $PM_{2.5}$. There are several difficulties in measuring $PM_{2.5}$ as well as PM_{10} (see Chapter 3) leading to a large uncertainty in the measurements.

7.4 Discussion of the assimilation results

A one year record of MODIS AOT data was assimilated into the LOTOS-EUROS model system using an ensemble Kalman filter. By itself this is a unique achievement and has never been done before. The results of the study should be regarded as an initial step for making particulate matter maps over Europe with more accurate and consistent concentrations. The whole procedure is associated with a few large uncertainties which are discussed below.

The model systematically underestimates observed AOT at AERONET sites, which is assumed to be the ground-truth. Verification of SO_4, NO_3 and NH_4 concentrations did not reveal large systematic deviations from observed concentrations and are probably not the cause for the underestimation of AOT. The systematic underestimation of the retrieved AOT data by the model can be explained by a number of factors.

(1) Missing sources. Reliable parameterizations for emissions of fugitive dust and SOA formation do not exist and are therefore not incorporated in the model. Furthermore, several sources are not very well known, e.g. anthropogenic combustion and biomass burning sources. This and a previous study (Schaap et al., 2004) indicated that the

concentrations of EC and OC are underestimated by a factor 2. Hence, the total fine aerosol concentration is underestimated and causes an underestimate of AOT.

(2) Limited vertical extent of the model. The vertical extent of the model is only 3.5 km, which also contributes to the underestimation of the AOT, as it is estimated that about 10 % of the aerosol is found above the model domain (Banic et al., 1996; Ten Brink et al., 2001, Builtjes et al, 2001).

(3) Uncertainty in aerosol optical properties. The model generally underestimates $PM_{2.5}$ by about 30%. However, modelled AOT may be underestimated by as much as 60%, or in some cases be within 20% of the observed value. Hence, the AOT calculation from the separate aerosol components was also identified to be a major source of uncertainties. The assumptions on optical properties, water uptake and (BC) mixing state have a large influence on the effective extinction coefficient. For example, using the AOT computation method developed in the ARIA2 project by Henzing (2006) yields 30 % lower AOT values than the method used in this study. Moreover, the hydration process, and thus the particle size distribution depends non-linearly on the relative humidity, a quantity that is very variable both in time and space. It is recommended to investigate the variability in calculated AOT between several methods currently in use by European modelling groups to assess AOT from modelled aerosol concentrations.

One of the most important conclusions of the ARIA-2 project (Verver et al., 2006) was that validation of satellite products, representation error and cloud contamination need to be addressed carefully. This study has build on this recommendation and evaluated the MODIS AOT data carefully against AERONET. In Chapter 5, it was shown that the MODIS AOT data are biased high. Consequently, an average bias correction was introduced. However, the uncertainty in the retrieved AOT is still rather high. Furthermore, our simple bias correction does not affect spatial patterns and, therefore, grids with erroneous AOT retrievals (not as such recognized by the retrieval scheme) are still included in the system. It is well known that AOT values above surfaces with a high albedo are very uncertain and difficult to detect. In this respect clouds are most important. Undetected cloud contamination yields an unknown overestimate of AOT. Furthermore, AOT values over shallow waters and over regions covered with snow are usually biased high. The data for Scandinavia in spring may be biased high for this reason. Consequently, shorelines and the large mountain ranges can often be recognized in AOT maps.

For the AOT retrieval from MODIS, assumptions are made on the aerosol mixture that contributes to the AOT. The retrieval algorithm necessarily assumes that the total AOT is determined by a combination of several aerosol types of aerosol, e.g., anthropogenic and sea salt aerosol. When other types dominate this may introduce errors in the retrievals.

It is estimated that only a (small) part of the systematic difference between the modelled and retrieved AOT values is due to the uncertainties in the traditional emissions of the precursors for acidifying components. However, the LOTOS-EUROS system uses these emissions to close the complete gap between measured and observed data. Hence, the estimated emission changes do not yield realistic values, although after assimilation the AOT values are in better agreement with independent surface observations. The high corrections indicate that it is needed to improve the modelling of the total aerosol mass and the calculation of aerosol optical thickness from the aerosol components. Also, the assimilation study should be regarded as a study to optimize the assessment of the atmospheric state instead of a parameter estimation study. In this respect the study may be compared to a re-analysis study in meteorology. To improve the effectiveness of the assimilation noise factors could be added to

the boundary conditions and meteorological parameters (such as rain fall), or to the aerosol optical properties.

In short, assimilation of MODIS AOT_F in LOTOS-EUROS leads to AOT fields that are in better absolute agreement with the measurements. This might be expected, given the large bias in the modelled AOT values. Since the gap between modelled and measured AOT is probably not primarily caused by uncertainties in the emissions of primary $PM_{2.5}$, SO_2, NO_x, VOC, and NH_3, not much value is attributed to the estimated updates of the emissions of these components resulting from the assimilation. The gap between modelled and measured AOT may be explained by a combination of missing aerosol components, uncertain emissions, limited vertical extent of the model, and the uncertainties in the calculation of the AOT from the single aerosol components. Hence, there are still many problems to be solved in the modelling of AOT, and also detailed evaluation of the retrieved AOT from the satellite instrument is indispensable.

It has been shown, however, that the assimilation system does work and most important improvements are in the timing and representation of spatial patterns of $PM_{2.5}$. The spatial correlation for $PM_{2.5}$ is 0.88 for the modelled field, and increases to 0.91 for the field based on the assimilation of AOT. $PM_{2.5}$ levels are also increased through the assimilation of MODIS AOT_F, by 2-3 $\mu g/m^3$ in central Europe. In conclusion, the assimilation of AOT provides a better agreement with the ground based measurements of $PM_{2.5}$, although still large absolute differences exist. The number of stations in Europe measuring $PM_{2.5}$ and the quality of these measurements should increase considerably to enable proper validation of assimilated $PM_{2.5}$ levels.

8. Discussion and conclusions

The understanding of particulate matter levels over Europe as a whole is at present limited by the diversity of ground level measurements methods. In this study the relation has been explored between satellite observations of aerosol optical thickness and concentrations of particulate matter at ground level for Europe in 2003. As such it aims to form an initial step for making particulate matter maps over Europe with more accurate and consistent concentrations.

AOT validation results

The AOT data as measured by the MODIS instruments on board the EOS/Terra and EOS/Aqua platforms, have been compared to AOT measurements of the AERONET surface network. The spatial correlation between MODIS and AERONET observed yearly average AOT over Europe is 0.64 for AOT and 0.72 for AOT_F. The temporal correlation between MODIS and AERONET observed AOT is generally high, with a mean correlation of 0.72 (0.77 median of all stations), with slightly lower correlation for the AOT_F. However, the results show that MODIS systematically overestimates the AOT. On average, the annual mean AOT (AOT_F) observed by MODIS across all validation stations is 0.30 (0.25) compared to 0.20 as obtained by the sun-photometers. A more or less constant bias was found between MODIS AOT and AOT_F and AERONET, of 0.7 and 0.9, respectively. After correction of the AOT and AOT_F values, through multiplication with 0.7 and 0.9, respectively, the MODIS data agree with AERONET within an uncertainty range of $\pm 0.05 \pm 0.2 AOT_F$.

Comparison of spatio-temporal variations of AOT and PM

As a second step, a comparison was made between spatial and temporal variations of particulate matter as measured by surface air quality networks in Europe (AIRBASE database), and aerosol optical thickness. The MODIS measurements clearly show the major aerosol source regions in Northern Italy, Southern Poland, and the Belgium/Netherlands/Ruhr area, as well as individual large cities and industrialized valleys (Rhone, Danube). The spatial correlation between yearly average PM_{10} and AOT is 0.58, based on 142 rural background stations across Europe. $PM_{2.5}$ shows spatial correlations of 0.77 with the fine fraction of the AOT, but this is limited to only 8 rural background stations that are available in AIRBASE for 2003. For $PM_{2.5}$, the spatial correlation is higher with the fine fraction of the AOT (AOT_F) than with the total AOT, while for PM_{10} the opposite is true. Temporal correlations of AOT or AOT_F with PM are similar.

While monthly average AOT and PM values both show clear anti-correlation with rainfall, the seasonal variation of AOT and PM is distinctly different. Throughout most of Europe, the AOT has a clear minimum in the winter months. The seasonal variation in PM differs across Europe, and at many locations the seasonal variation is less marked than that of the AOT. A plausible explanation is that high precipitation in winter leads to lower aerosol burdens (hence, lower AOT and PM), but this is to some extent offset by lower boundary layer heights in winter, which lead to higher PM concentrations near the surface but do not affect the AOT. Consequently, the correlation between one-year time-series of AOT with PM_{10} or $PM_{2.5}$ is low (0.3). The correlation between PM and AOT is enhanced when the AOT is divided by the boundary layer height and, to a lesser extent, when it is corrected for growth of aerosols with relative humidity. In that case, the average time-correlation is 0.5 (PM_{10}) and

0.6 ($PM_{2.5}$), averaged over all rural background stations with more than 50 data-pairs per time-series.

This scaling of the AOT with boundary layer height and relative humidity substantially improves the time-correlation with PM, as day-to-day variations in boundary layer height and relative humidity influence PM and AOT levels. However, this scaling does not improve the spatial correlation of the yearly averages. The reason is that yearly average boundary layer height or atmospheric humidity is not clearly related to PM concentration levels. For example, the boundary layer is, on average, higher in Southern Europe than in Northern Europe, while AOT and PM levels do not show corresponding lower PM or AOT levels in Southern Europe.

Statistical mapping results

A map of yearly average concentrations of $PM_{2.5}$ has been constructed, through fitting modelled $PM_{2.5}$ and measured AOT_F fields to observed $PM_{2.5}$ concentrations.The LOTOS-EUROS model has been used to for the modelled PM 2.5 concentrations For this fitting, in the final stage of this study, also five EMEP stations were added to the eight rural background stations in the AirBase database, to obtain a more uniform spatial coverage within the fitting domain (Europe). Using both modelled $PM_{2.5}$ and measured AOT_F fields as explanatory variables for the yearly average $PM_{2.5}$ distribution, the RMS-errors decrease by about 25% compared to fitting with only one explanatory variable. The spatial correlation between fitted and observed yearly average $PM_{2.5}$ levels is 0.82, with a RMS-error of 2.8 $\mu g/m^3$. Since the modelled $PM_{2.5}$ and measured AOT_F fields contribute about equally to the fitted map, the fitted map resembles the features of the modelled $PM_{2.5}$ map and the AOT_F map in equal proportions. The number of stations considered in this fitting is limited however, and adding more stations may significantly alter the resulting map, depending on where these stations are located. For example, the gradient in AOT_F between Scandinavia and Spain appears not very realistic, with higher AOT_F-values in Scandinavia than in Spain. This gradient is opposite (and more realistic) in the modelled field. Therefore, adding more stations in Scandinavia and Spain will reduce the weight attached to the AOT_F-field and increase that attached to the modelled field.

Assimilation results

The assimilation was performed with a LOTOS-EUROS model version that was slightly updated to that used in the statistical fitting approach. Also, the assimilation has been done for a more limited area to speed up calculation time. The assimilation of MODIS AOT_F in LOTOS-EUROS leads to AOT fields that are in better agreement with the measurements. It was shown that the assimilation system does work and most important improvements are in the timing and representation of spatial patterns in AOT. $PM_{2.5}$ levels are increased through the assimilation of MODIS AOT_F by 2-3 $\mu g/m^3$ in central Europe. The assimilation also slightly increases the spatial correlation between measured and modelled yearly average $PM_{2.5}$ (from 0.88 to 0.91).

In the assimilation, the emissions (primary and precursors of secondary aerosols) have been taken as free parameter. Therefore, the assimilation has little effect for areas with low emissions. As a result of the assimilation, changes in the emission strengths are found. However, not much value is attributed to this, as the differences between model and measurements are too large. The absolute bias is not only attributable to emissions that are absent in the emission inventories, but also to errors in the description in the chemical transformation, dispersion and deposition of aerosols. Moreover, there is a large uncertainty

in the optical properties of the aerosols that determine the relationship between PM and AOT. Another approach would have been to take as free parameter optical properties of the aerosols, which are also very uncertain.

Comparison between statistical mapping and assimilation approach

Generally, the features in the map based on the statistical mapping approach resemble that of the assimilation approach in the central part of the model domain (see Figure 8.1). It is apparent that the relative difference between the two approaches is particularly large near the boundaries of the model domain. This is caused by taking the boundary conditions fixed, which causes little difference between various members in the ensemble used for the Kalman filter. This leads to less noise in the modelled results near the boundaries, and hence, much weight to the modelled field. Another reason is that the emissions are rather low at most of the boundaries, which leads to little influence of adjusting the emissions in these areas. Also it is apparent that the differences are large in Scandinavia. This points at overestimated AOT values by MODIS. In the current statistical approach, the weight given to the AOT map and the modelled $PM_{2.5}$ map is constant over Europe, and if the AOT is overestimated in one region, this shows up in the resulting fitted field. It also means that in the statistical approach, a spatially uniform relationship is applied to convert AOT to PM. In reality, this relationship will depend on the aerosol chemical composition which determines e.g. hygroscopic and optical properties. In the assimilation approach, the relation between AOT and PM depends on the modelled aerosol properties.

It is also apparent that the assimilation approach leads to lower $PM_{2.5}$ concentrations than the statistical mapping approach. The absolute difference is 2-3 $\mu g/m^3$ in the centre of the domain and increases to 5-7 $\mu g/m^3$ near the boundaries of the domain. In the statistical mapping approach, the absolute measured levels of the $PM_{2.5}$ are actively used in the mapping procedure, in contrast to the assimilation approach where $PM_{2.5}$ measurements are used only for validation. Because of this, the statistical mapping approach leads by definition to no bias compared to the ground-based measurements, while data-assimilation will provide a bias depending on the model underestimation of PM, the uncertainty in the conversion between AOT and PM, and the uncertainty assumed for the AOT data and model results. In the assimilation approach, the remaining bias between assimilated and measured PM2.5 is 5.2 $\mu g/m^3$ while it is 4.0 $\mu g/m^3$ without assimilation.

Both methods lead to better description of the spatial gradients in the yearly average $PM_{2.5}$ field in Europe as compared to modelled results only. In the assimilation approach, the spatial correlation between yearly average $PM_{2.5}$ measurements and the assimilated $PM_{2.5}$ field was already high (0.88) in the area considered, and increases to 0.91 after assimilation, while in the statistical approach, which is applied to a larger domain and with a slightly different model version, it increases from 0.70 to 0.82. Largest uncertainties in both methods are related to missing aerosol sources and the optical properties of aerosols that determine the relation between AOT and PM. The relation between AOT and PM will be addressed in the follow-up project SATLINK (Linking Satellite Observations of Aerosol Optical Depth with Ground Level Observations of Particulate Matter). Highest concentrations of $PM_{2.5}$ are found in densely populated and industrialized areas, such as the Po-valley, the Benelux countries, the Ruhr area, areas in Central Europe and specific large cities in Europe.

In this study, the $PM_{2.5}$ data were used ‘as is’, i.e. directly taken from the AirBase (or EMEP) databases without paying attention to correction factors. Hence, any artefacts in the measured $PM_{2.5}$ levels stemming from inaccurate calibration will also show up in the fitted fields. The

assimilated fields are not affected by this, as the measured $PM_{2.5}$ data are only used for validation. It may therefore have affected correlation statistics between assimilated $PM_{2.5}$ and observed $PM_{2.5}$. For PM_{10}, it is well known that calibration factors differ between different air quality networks (Buijsman and de Leeuw, 2004). Van de Kassteele et al. (2006) have developed a statistical mapping approach in which possible systematic differences between countries were taken into account for PM_{10}, under the assumption that the explanatory fields do not have artificial systematic differences between countries. Since it is not clear whether this assumption is really true, a simpler statistical mapping method ignoring possible calibration artefacts is used here.

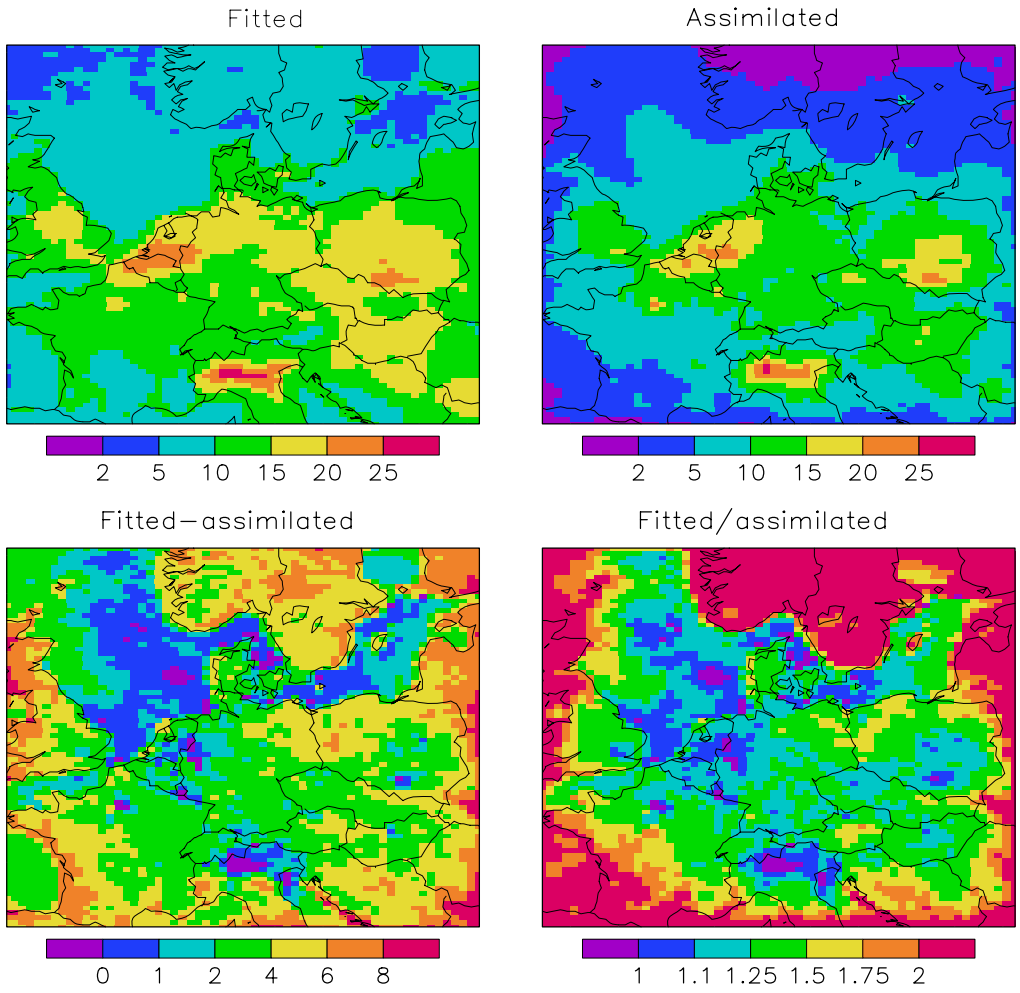

Figure 8.1 Fitted (upper, left) and assimilated (upper, right) fields of $PM_{2.5}$, their absolute difference in $\mu g/m^3$ (bottom, left) and their ratio (bottom, right).

Measurement strategy how satellite observations may improve air quality mapping

The impact of satellite observations on air quality mapping, in this case mapping of ground level $PM_{2.5}$ concentrations, obviously depends on the amount of ground level observations, and the amount of satellite AOT values. In the extreme case that over Europe in every grid cell of 10 x 10 km2 a $PM_{2.5}$ ground level observation on an hourly basis, and with perfect QA/QC over all of Europe would exists, the impact of having in addition AOT observations would obviously be minimal. It is also clear that in areas without $PM_{2.5}$ ground level observations, so in 2003 in large parts of Southern and Eastern Europe (see Fig 3.2), the

impact of AOT observations in being able to derive ground level $PM_{2.5}$ concentrations in these areas is substantial. The system which has been further developed and applied in this study consisting of the LOTOS-EUROS model and the data assimilation method ensemble Kalman filtering makes it in principle possible to quantify the relative impact of ground level and AOT observations in mapping $PM_{2.5}$ air quality and to derive information about measuring strategies.

At the moment with AOT from MODIS, the clear disadvantage relative to ground level observations, especially hourly data, is the fact that at maximum there are 2 observations of AOT per day, and then only under cloud-free conditions. Assuming a cloud-cover of on average 50 % , AOT observations cover only 5 % of the time that ground level observations are available. This limited time resolution clearly limits the usefulness of the AOT data. Furthermore, total column AOT-values have to be translated to ground level observations, using a number of assumptions, (see e.g., Chapter 7), which results in a relatively large error range, also decreasing the impact of AOT-data. In case AOT observations would be performed more frequently, like hourly, the impact would be larger. Hourly AOT-observations are however only possible using Geostationary Satellites.

In a recent, and still ongoing study funded by EUMETSAT, Darmstadt, TNO has performed a so-called Observing System Simulation Experiment, OSSE, to determine the impact of hourly AOT observations by a Geostationary Satellite relative to ground level observations. The OSSE is performed by using the LOTOS-EUROS with the Ensemble Kalman filter data assimilation. Preliminary results indicate the large impact of total hourly to 4-hourly AOT observations in especially the south of Europe, an area with limited ground level observations. Under investigation is also whether vertical profile observations of AOT, with 2 km resolution, would be beneficial to detect aerosol layers aloft, coming for example from Saharan Dust (Timmermans et al, 2006).

Cost-benefit analysis

For end-users, there are no costs for the acquisition of MODIS satellite data of aerosol optical thickness. Nevertheless, the processing of the data is a non-trivial task, as the data volumes are high: one year of MODIS Terra and Aqua AOT data for Europe amounts to 150 Gigabyte. Current PCs are well capable of processing such amounts of data, and costs related to sufficient hard-disks storage capacity is limited to a few hundred Euro. The processing also requires maintenance of read-in software (HDF-format), elementary quality control and data-processing (level 2 to 3) software. Also costs are related to model development, running the model and analysing the result. Clearly, project costs are dominated by personal costs. Within the PARMA project, software has been developed. Re-analysing the study with another year, and assuming that no further adoptions to the software would be necessary, i,e., marginal costs, would take probably a few months of work (combining the statistical mapping and the data-assimilation approach). The benefits of this work are improved maps of $PM_{2.5}$, and improved insight in the quality of measuring and modelling AOT and $PM_{2.5}$. The results of this work have been presented at various meetings and have in part been published in the reviewed literature (see outreach activities and publications). It is hard to quantify the benefits in monetary terms, however.

Acknowledgements

The MODIS data were kindly made available by the NASA staff. We acknowledge all scientists that submitted their data to the AirBase database, and those maintaining the AirBase database. We would like to thank our colleagues Liesbeth de Waal and Ferd Sauter for assisting us reading the MODIS data files, and Patrick van Hooydonck for his assistance with extracting particulate matter data from AirBase. We thank all Aeronet instrument PI's that submitted their data in the Aeronet database.

Outreach activities and publications

Various aspects of the work were presented at various meetings, among which:

- Homan, C.D. 'Modis aerosol optical thickness over Europe compared to surface PM data', 5th urban air quality conference, Valencia, March 2005.
- Koelemeijer, R.B.A. 'Detection of particulate matter over Europe with Modis', KNMI, June 2005.
- Koelemeijer, R.B.A. 'Het gebruik van satelliet aërosol metingen voor PM', VVM-symposium luchtkwaliteit en satellieten, June 2006.
- Timmermans, R.M.A. 'Satellietmetingen van aërosolen - validatie', VVM-symposium luchtkwaliteit en satellieten, June 2006.
- Schaap, M. 'Data assimilatie van satelliet aërosol metingen', VVM-symposium luchtkwaliteit en satellieten, June 2006.

The following publications were made within the framework of PARMA project:

- Homan, C.D., R.B.A. Koelemeijer, and J. Matthijsen, 2005. Modis aerosol optical thickness over Europe compared to surface PM data, proceedings of the 5th Air Quality Conference, Valencia, march 2005, on CDROM.
- Koelemeijer, R.B.A., Homan, C.D., and Matthijsen, J., 2006. Comparison of spatial and temporal variations of aerosol optical thickness and particulate matter in Europe, *Atmospheric Environment*, 40, 5304-5315.
- Van de Kassteele, J., Koelemeijer, R.B.A., Dekkers, A.L.M., Schaap, M., C. D. Homan, C.D., Stein, A., 2006. Statistical mapping of PM10 concentrations over Western Europe using secondary information from dispersion modelling and MODIS satellite observations, *Stochastic Environmental Research and Risk Assessment,* DOI 10.1007/s00477-006-0055-4.
- Van de Kassteele, J., 2006. Statistical PM10 mapping using dispersion modelling and satellite observations, in: *Statistical Air Quality Mapping,* PhD thesis Wageningen University, 140 pp.

References

- Adelman, Z.E., 1999. A re-evaluation of the Carbon Bond-IV photochemical mechanism. M.Sc. thesis, Department of Environmental Sciences and Engineering, School of Public Health, University of North Carolina, USA.
- Banic, C.M., W.R. Leaitch, G.A. Isaac, M.D. Couture, L.I. Kleinman, S.R. Springston, and J.I. MacPherson, 1996. Transport of ozone and sulfur to the North Atlantic atmosphere during the North Atlantic Regional Experiment. J. Geophys. Res. 101, D22, 29091-29104
- Brunekreef B. and Holgate, S.T., 2002. Air pollution and health. The Lancet 360, 1233-1242.
- Buijsman, E. en F.A.A.M. De Leeuw, 2004. PM_{10} measurement results and correction factors in AirBase, ETC/ACC Technical Paper 2004/4, European Topic Centre on Air and Climate Change, Bilthoven.
- Builtjes P.J.H., van Loon M., Schaap M., Teeuwisse S., Visschedijnk A.J.H., Bloos J.P., 2003. Project on the modelling and verification of ozone reduction strategies: contribution of TNO-MEP, TNO-report MEP-R2003/166, TNO, Apeldoorn.
- Builtjes, P.J.H., H.M. ten Brink, G. de Leeuw, M. van Loon, C. Robles Gonzales, M. Schaap, 2001. Aerosol air quality satellite data, BCRS USP-2 report 00-33, Apeldoorn.
- CAFE-Working Group on Particulate Matter, 2004. Second Position Paper on Particulate Matter. See http://europa.eu.int/comm/environment/air/cafe/.
- Chu, D.A., Y. J. Kaufman, C. Ichoku, L.A. Remer, D. Tanré and B.N. Holben, 2002. Validation of MODIS aerosol optical thickness retrieval over land, Geophys. Res. Lett., 29, NO. 12, doi:10.1029/2001GL013205.
- Chu, D.A., Y.J. Kaufman , G. Zibordi, J.D. Chern, J. Mao, C. Li, and B.N. Holben, 2003. Global monitoring of air pollution over land from the Earth Observing System-Terra Moderate Resolution Imaging Spectroradiometer (MODIS), J. Geophys. Res., 108, 4661, doi:10.1029/2002JD003179.
- Charron, A., R.M. Harrison, S. Moorcroft, J. Booker, 2004. Quantitative interpretation of divergence between PM_{10} and $PM_{2.5}$ mass measurement by TEOM and gravimetric (Partisol) instruments, Atmos. Env., 38, 415-423.
- Day, D.E. and W.C. Malm, 2001. Aerosol light scattering measurements as a function of relative humidity: a comparison between measurements made at three different sites, Atmos. Env., 35, 5169-5176.
- Dockery D.W., Pope III, C.A., Xu, X., Spengler, J.D., Ware, J. H., Fay, M.E., Ferris, B.G. and Speizer, F.E., 1993. An Association between Air Pollution and Mortality in Six U.S. Cities. The New England Journal of Medicine 329, 1753-1759.
- EN 12341, 1998. Air Quality – Determination of the PM10 fraction of suspended particular matter – Reference method and field test procedure to demonstrate equivalence of measurement methods.
- Fitzgerald, J. W.: Dependence Engel-Cox, J.A., Holloman, C.H., Coutant, B.W. and Hoff, R.M., 2004. Qualitative and quantitative evaluation of MODIS satellite sensor data for regional and urban scale air quality, Atmospheric Environment 38, 2495-2509.
- Erisman, J.W., van Pul, A., Wyers, P., 1994. Parametrization of surface-resistance for the quantification of atmospheric deposition of acidifying pollutants and ozone, Atmos. Environ., 28, 2595-2607
- EU, 1996. Council Directive 96/62/EC of 27 September 1996 on ambient air quality assessment and management. Official Journal L 296 , 21/11/1996.

- EU, 1999. Council Directive 1999/30/EC of 22 April 1999 relating to limit values for sulphur dioxide, nitrogen dioxide and oxides of nitrogen, particulate matter and lead in ambient air, Official Journal L 163 , 29/06/1999.
- Evensen, G., 1997. Advanced data assimilation for strongly nonlinear dynamics. Monthly Weather Review 125, 1342-1354.
- Hansen J. E. and Sato M., 2001. Trends of measured climate forcings agents, Proc. Nat. Acad. Sci., 98, 14778-14783.
- Henzing, J.S. 2006. Aerosol modelling spatial distributions and effects on radiation, Ph.D thesis Techn.Univ Eindhoven.
- Hitzenberger, R., A. Berner, Z. Galambos, W. Mauenhaut, J. Cafmeyer, J. Schwarz, K. Müller, G. Spindler, W. Wieprecht, K. Acker, R. Hillamo, and T. Mäkelä, 2004. Intercomparison of methods to measure the mass concentration of the atmospheric aerosol during INTERCOMP2000- influence of instrumentation and size cuts, Atmos. Env., 38, 6467-6476.
- Hodzic, A., R.Vautard, H.Chepfer, P. Goloub, L. Menut, P. Chazette, J.L. Deuzé, A. Apituley, and P. Couvert, 2005. Evolution of aerosol optical thickness during the August 2003 heat wave as seen from CHIMERE model simulations and POLDER data, Atmos. Chem. Phys. Discuss, 5, 4115-4141.
- Hutchison, K.D., 2003. Applications of MODIS satellite data and products for monitoring air quality in the state of Texas. Atmospheric Environment 37, 2403-2412.
- Ichoku, C., Remer, L.A., and Eck, T.F., 2005. Quantitative evaluation and intercomparison of morning and afternoon Moderate Resolution Imaging Spectroradiometer (MODIS) aerosol measurements from Terra and Aqua. J. Geophys. Res. 110, D10S03, doi:10.1029/2004JD004987.
- IPCC, 200. Climate change 2001: The Scientific Basis, Contribution of Working group I to the third assessment report of the IPCC, Houghon et al. (eds), Cambridge, 881 pp.
- Kaufman, Y.J. and D. Tanré, 1998. Algorithm for Remote Sensing of Tropospheric Aerosol from MODIS, Product ID MOD04.
- Kerschbaumer and Reimer, 2003. Meteoroloical data preparation for the Rem/CALGRID model. UBA-projetc 29943246, Freie Univ. Berlin.
- Kiehl, J. T., and B. P. Briegleb, 1993,The relative roles of sulfate aerosols and greenhouse gases in climate forcing, Science, 260, 311-314.
- Kinne S., U. Lohmann, J. Feichter, M. Schulz, C. Timmreck, S. Ghan, R. Easter, M. Chin, P. Ginoux, T. Takemura, I. Tegen, D. Koch, M. Herzog, J. Penner, G. Pitari, B. Holben, T. Eck, A. Smirnov, O. Dubovik, I. Slutsker, D. Tanre, O. Torres, M. Mischenko, I. Geogdzhayev, D.A. Chu, and Y. Kaufman, 2003. Monthly averages of aerosol properties: A global comparison among models, satellite data, and AERONET ground data, J. of Geoph. Res., 108, NO. D20, 4634, doi: 10.1029/2001JD001253.
- Knol A.B. and Staatsen, B.A.M., 2005. Trends in the environmental burden of disease in the Netherlands 1980-2000, RIVM report 500029001, RIVM, Bilthoven.
- Koelemeijer, R.B.A., Homan, C.D., and Matthijsen, J., 2006. Comparison of spatial and temporal variations of aerosol optical thickness and particulate matter in Europe, Atm. Env. 40, 5304-5315.
- Liu and Durran, 1977. The development of a regional air pollution model and its application to the Northern Great Planes, EPA-908/1-77-001, p. 281 SAI, San Rafael, California.
- Logan, J., 1998. An analysis of ozonesonde data for the troposphere, recommendations for testing 3-D models and development of a gridded climatology for tropospheric ozone, J. Geophys. Res. 104, 16.

- Mie, G., Beiträge zur optik trüber medien, speziell kolloidaler metallösungen, Ann. Phys., Leipzig, 25, 377-445, 1908.
- Monahan, E.C., Spiel, D.E., Davidson, K.L., 1986. A model of marine aerosol generation via whitecaps and wave disruption, In Oceanic Whitecaps and their role in in air/sea exchange, edited by Monahan, E.C, and Mac Niocaill, G., pp. 167-174, D. Reidel, Norwell, Mass., USA
- Nenes, A., Pilinis, C., and Pandis, S. N.,1999. Continued Development and Testing of a New Thermodynamic Aerosol Module for Urban and Regional Air Quality Models, Atmos. Env. 33, 1553-1560
- Pope III, C.A., Dockery, D.W., Schwartz, J., 1995. Review of epidemiological evidence of health effects of particulate air pollution. Inhalation Toxicology 7, 1–18.
- Pope III, C.A.., Burnett, R.T., Thun, M.J., Calle, E.E., Krewski, D, Ito, K., Thurston, G.D., 2002. Lung Cancer, Cardiopulmonary Mortality, and Long-term Exposure to Fine Particulate Air Pollution, J. Am. Med. Assoc. 287, 1132-1141.
- Poppe, D., Y. Andersson-Sköld, A. Baart, P.J.H. Builtjes, M. Das, F. Fiedler, O. Hov, F. Kirchner, M. Kuhn, P.A. Makar, J.B. Milford, M.G.M. Roemer, R.Ruhnke, D. Simpson, W.R. Stockwell, A. Strand, B. Vogel, H. Vogel, 1996. Gas-phase reactions in atmospheric chemistry and transport models: a model intercomparison. Eurotrac report. ISS, Garmisch-Partenkirchen.
- Querol X., A . Alastuey, C.R. Ruiz, B. Artinano, H.C. Hansson, R.M. Harrison, E. Buringh, H.M. ten Brink, M. Lutz, P. Bruckmann, P. Straehl, J. Schneider, 2004. Speciation and origin of PM10 and PM2.5 in selected European cities, Atmos. Environ., 38, 6547-6555.
- Remer, L.A., Y.J. Kaufman, D. Tanré, S. Mattoo, D.A. Chu, J.V. Martins, R.-R. Li, C. Ichoku, R.C. Levy, R.G. Kleidman, T.F. Eck, E. Vermote, and B.N. Holben, 2005. The MODIS Aerosol Algorithm, Products, and Validation, J. Atmos. Sci., 62, 947-973.
- Schaap, M., Dernier Van Der Gon, H.A.C., Dentener, F.J., Visschedijk, A.J.H., Van Loon, M., Ten Brink, H.M., Putaud, J.-P., Guillaume, B. Liousse, C., and Builtjes, P.J.H., 2004. Antropogenic black carbon and fine aerosol distribution over Europe. J. Geophys. Res. 109, D18207, doi:10.1029/2003JD004330.
- Schaap, M., Roemer, M. Sauter, F. Boersen, G., Timmermans, R., Builtjes, P.J.H., 2005a. LOTOS-EUROS: Documentation, TNO-report B&O-A R 2005/297, TNO, Apeldoorn.
- Schaap, M. Sauter, F., Timmermans, R.M.A., Roemer, M., Velders, G., Beck, J., and Builtjes, P.J.H., 2005b. The LOTOS-EUROS model: description, validation and latest developments, Int. J. of Environment and Pollution, accepted.
- Simpson, D., Fagerli, H., Jonson, J.E., Tsyro, S., Wind, P., and Tuovinen, J-P., 2003. Transboundary Acidification, Eutrophication and Ground Level Ozone in Europe, Part 1: Unified EMEP Model Description, EMEP Report 1/2003, Norwegian Meteorological Institute, Oslo, Norway
- Tang, I. N., 1997. Thermodynamic and optical properties of mixed-salt aerosols of atmospheric importance, J. Geophys. Res., 102, D2, 1883–1893.
- Tegen, I., P. Hollrig, M.Chin, I. Fung, D. Jacob, J. Penner, 1997, Contribution of different aerosol species to the global aerosol extinction optical thickness: Estimates from model results. J. Geophys. Res. 102, 23,895-23,915.
- Ten Brink H. M., Hensen, A., Khystov, A., van Dorland, R., Jeuken, A., van Velthoven, P., Lelieveld, J., van den Berg, A., Swart, D.P.J., Bergwerff, J.B., Apituley, A., 2001. Aerosol; cycle and influence on the radiation balance, Cluster-project in the National Research Program on Global Air Pollution and Climate Change, npr2, ECN report 410200064, ECN, Petten.

- Timmermans, R.M.A., M. Schaap, P.J.H. Builtjes, R. Siddans, 2006. The operational use of satellite derived aerosol information to assess fine particulate matter concentrations over Europe, TNO-report 2006-A-R0309-B, TNO, Apeldoorn.
- Van de Hulst, 1981. Light scattering by small particles, ISBN 0-486-64228-3, Dover Publications, New York.
- Van de Kassteele, J., Koelemeijer, R.B.A., Dekkers, A.L.M., Schaap, M., C. D. Homan, C.D., Stein, A., 2006. Statistical mapping of PM10 concentrations over Western Europe using secondary information from dispersion modelling and MODIS satellite observations, Stochastic Env. Research and Risk Assessment, DOI 10.1007/s00477-006-0055-4.
- Van Loon, M, P.J.H. Builtjes, A.Segers, 2000. Data assimilation of ozone in the atmospheric transport chemistry model LOTOS, Env. Modelling and Software 15, 603-609.
- Veefkind J.P., J.C.H. van der Hage, and H. M. ten Brink, 1996. Nephelometer derived and directly measured aerosol optical thickness of the atmospheric boundary layer, Atmos. Res., 41, 217-228.
- Veefkind, J.P., 1999. Aerosol Satellite Remote Sensing. PhD-thesis, Univ. Utrecht.
- Veldt, C. 1991. The use of biogenic VOC measurements in emission inventories, MT-TNO Report 91-323, TNO, Apeldoorn.
- Verver G.H.L., J.S. Hensing, M. Schaap, P.J.H. Builtjes, P.F.J. Velthoven, R. Schoemaker, G. de Leeuw, 2006. Aerosol Retrieval and Assimilation phase 2 (ARIA-2). NIVR-Rep.
- Visschedijk, A.J.H. and H.A.C. Denier van der Gon, 2005. Gridded European anthropogenic emission data for NOx, SOx, NMVOC, NH3, CO, PM 10, PPM 2.5 and CH4 for the year 2000. TNO-Rep B&O-A R 2005/106, TNO, Apeldoorn.
- Walcek,C.J. 2000. Minor flux adjustment near mixing ration extremes for simplified yet highly accurate monotonic calculation of tracer advection. J. Geophys. Res. 105, D7, 9335-9348.
- Wang J. and Christopher, S.A. 2003. Intercomparison between satellite-derived aerosol optical thickness and PM2.5 mass: implications for air quality studies. Geophys. Res. Lett., 30 (21), 2095, doi:10.1029/2003GL018174.
- Whitten G., Hogo, H., Killus, J., 1980. The Carbon Bond Mechanism for photochemical smog, Env. Sci. Techn. 14, 14690-700.
- Yamartino R.J., J. Flemming, R.M. Stern., 2004. Adaption of analytic diffusivity formulation to Eulerian grid model layers of finite thickness, 27th NATO/CCMS ITM on air pollution modelling and its application, Banff.

Annex A: Comparison of MODIS and AERONET data

Table A.1 Comparison AERONET AOT observations with MODIS observations of AOT and AOT_F in Europe in 2003. Only stations are shown with more than 15 days with both MODIS and AEORNET data.

					Yearly average data			**Time correlations**	
country	**station**	**lon**	**lat**	**N**	**AERONET AOT**	**MODIS AOT**	**MODIS AOT_F**	**AERONET-MOD (AOT)**	**AERONET-MOD (AOT_F)**
Algeria	Blida	2.9	36.5	27	0.08	0.15	0.12	0.43	0.45
Belarus	Minsk	27.5	53.0	120	0.17	0.27	0.26	0.70	0.85
Belgium	Oostende	2.9	51.2	119	0.25	0.42	0.40	0.81	0.82
Estonia	Toravere	26.5	58.3	93	0.14	0.22	0.21	0.25	0.33
France	Avignon	4.9	43.9	262	0.18	0.31	0.28	0.80	0.79
France	Bordeaux	-0.6	44.8	18	0.11	0.15	0.13	0.89	0.87
France	Dunkerque	2.4	51.0	66	0.19	0.30	0.25	0.74	0.75
France	Fontainebleau	2.7	48.4	140	0.23	0.27	0.27	0.80	0.79
France	Lille	3.1	50.6	120	0.22	0.36	0.35	0.88	0.88
France	Palaiseau	2.2	48.7	142	0.24	0.30	0.31	0.77	0.74
France	Rossfeld	7.6	48.3	24	0.30	0.39	0.38	0.63	0.58
France	Toulouse	1.4	43.6	186	0.18	0.36	0.24	0.80	0.64
Germany	Hamburg	10.0	53.6	161	0.18	0.33	0.32	0.81	0.78
Germany	Helgoland	7.9	54.2	63	0.17	0.19	0.14	0.89	0.90
Germany	IFT-Leipzig	12.4	51.4	104	0.22	0.42	0.39	0.75	0.78
Germany	Munich Maisach	11.3	48.2	82	0.20	0.31	0.32	0.70	0.64
Greece	Forth Crete	25.3	35.3	242	0.19	0.40	0.15	0.51	0.53
Italy	Etna	15.0	37.6	93	0.23	0.35	0.27	0.83	0.46
Italy	IMC_Oristano	8.5	39.9	211	0.22	0.34	0.22	0.81	0.45
Italy	ISDGM CNR	12.3	45.4	251	0.24	0.51	0.43	0.81	0.85
Italy	Ispra	8.6	45.8	230	0.29	0.28	0.29	0.68	0.65
Italy	Lampedusa	12.6	35.5	154	0.21	0.25	0.15	0.91	0.87
Italy	Lecce University	18.1	40.3	223	0.20	0.29	0.25	0.76	0.62
Italy	Rome Tor Vergata	12.6	41.8	260	0.21	0.32	0.26	0.77	0.69
Italy	Venise	12.5	45.3	241	0.22	0.31	0.24	0.62	0.72
Moldova	Moldova	28.8	47.0	60	0.25	0.21	0.23	0.84	0.74
Netherlands	The Hague	4.3	52.1	75	0.24	0.34	0.33	0.91	0.91
Portugal	Evora	-7.9	38.6	121	0.14	0.26	0.09	0.83	0.55
Russia	Moscow	37.5	55.7	96	0.20	0.34	0.34	0.19	0.18
Spain	El Arenosillo	-6.7	37.1	241	0.14	0.29	0.23	0.82	0.75
Spain	Palencia	-4.5	42.0	144	0.14	0.32	0.10	0.59	0.10
Sweden	Gotland	19.0	57.9	115	0.12	0.24	0.24	0.77	0.77
Switzerland	Laegeren	8.4	47.5	46	0.13	0.18	0.18	0.50	0.45
Turkey	IMS METU	34.3	36.6	222	0.23	0.34	0.28	0.70	0.71
	Average				**0.20**	**0.30**	**0.25**	**0.72**	**0.66**
	Median				**0.20**	**0.31**	**0.26**	**0.77**	**0.73**

Annex B: Seasonal average maps of AOT_F

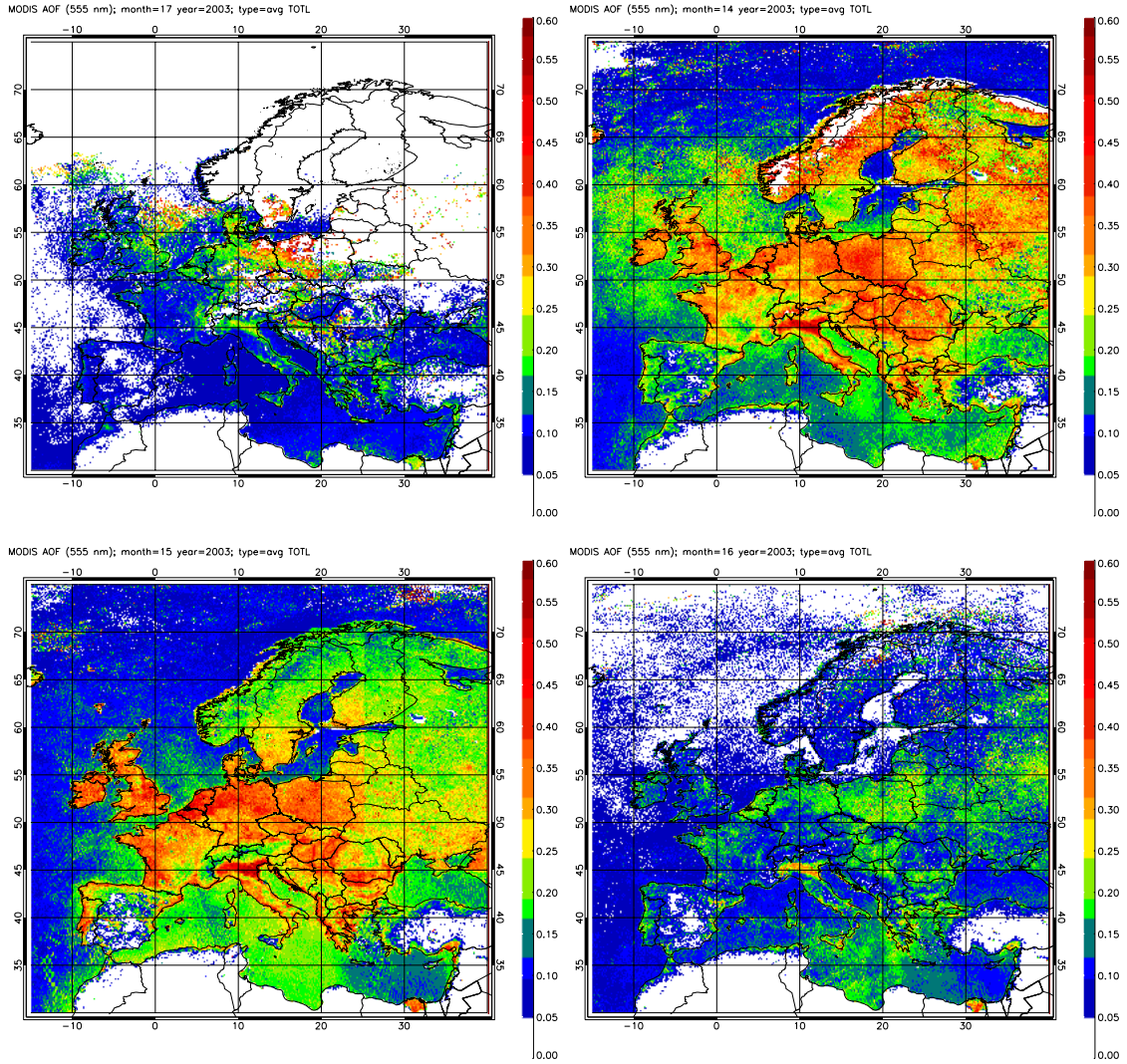

Figure B.1 Seasonal average maps of AOT_F. Top left: winter (DJF), top right: spring (MAM), bottom left: summer (JJA), top right: autumn (SON). Missing values are depicted in white.